Quantitative Structural Diagnosis of Plate-like Structures using Multi-frequency Lamb Wave Diffraction Tomography

Gnana Teja Pudipeddi

Thesis submitted in fulfilment of the requirements for the degree of Doctor of Philosophy

Faculty of Engineering, Computer and Mathematical Sciences

School of Civil, Environmental and Mining Engineering

The University of Adelaide

July, 2019

Dedicated to my parents,

P. Jaya Bhargavi and P.V.S.S Subrahmanyam

Quantitative Structural Diagnosis of Plate-like Structures using Multi-frequency Lamb Wave Diffraction Tomography

By:

Gnana Teja Pudipeddi

Supervised By:

Associate Professor Ching-Tai Ng, *Ph.D.*,
School of Civil, Environmental and Mining Engineering,
The University of Adelaide

Professor Andrei Kotousov, *Ph.D.*,
School of Mechanical Engineering,
The University of Adelaide

Thesis submitted in fulfilment of the requirements for the degree of
Doctor of Philosophy
School of Civil, Environmental and Mining Engineering
Faculty of Engineering, Computer and Mathematical Sciences
The University of Adelaide
North Terrace, Adelaide, SA, 5005, Australia
Tel: +61(8) 8303 4323
Fax: +61(8) 8303 4359
Email: gnanateja.pudipeddi@adelaide.edu.au

Abstract

Quantitative identification and evaluation of damage are of utmost importance for the safety and sustainability of a structure. Identifying early stage damage is also necessary for reducing the maintenance and repair costs of a structure and increasing its service life. Numerous Structural Health Monitoring (SHM) systems have been developed over time to address these issues in various capacities and prevent huge losses to life and economy.

Lamb Wave Diffraction Tomography (LWDT) is an advanced SHM process that is used for identifying the location and quantifying the severity of damage. The process consists of interrogating a region of probable damage with Lamb waves and gathering information about the presence and geometry of the damage from the scattered waves. This process can be used in plate-like structures, such as metallic plates and composite laminates. One of the main areas of research in LWDT is investigating the effects of multiple non-central frequency components of data on the image quality and utilizing information from these multiple frequencies to reconstruct the damage.

This thesis contains journal papers that 1) study the scattering of Lamb waves at delaminations within a composite laminate, focussing on the mode-conversion effect at the damage boundary 2) study the effects of non-central frequencies on the quality of imaging for damage reconstruction and 3) propose multi-frequency approaches that improve the efficiency of LWDT.

The key outcome of this study is that a multi-frequency approach to damage reconstruction greatly improves the resolution of damage in plate-like structures,

without increasing the number of transducers. A multi-frequency based reconstruction approach would thus lead to the advancement of LWDT as a feasible technique for the SHM of plate-like structures.

Declaration

I certify that this work contains no material which has been accepted for the award of any other degree or diploma in my name, in any university or other tertiary institution and, to the best of my knowledge and belief, contains no material previously published or written by another person, except where due reference has been made in the text. In addition, I certify that no part of this work will, in the future, be used in a submission in my name, for any other degree or diploma in any university or other tertiary institution without the prior approval of the University of Adelaide and where applicable, any partner institution responsible for the joint-award of this degree.

I acknowledge that copyright of published works contained within this thesis resides with the copyright holder(s) of those works. I also give permission for the digital version of my thesis to be made available on the web, via the University's digital research repository, the Library Search and also through web search engines, unless permission has been granted by the University to restrict access for a period of time.

I acknowledge the support I have received for my research through the provision of an Australian Government Research Training Program Scholarship.

Signed:……. Date:……

Acknowledgements

This thesis wouldn't have been possible without the selfless efforts of my supervisor, Dr Ching Tai-Ng (Alex). His advice and support at every stage of my research went above and beyond the requirements of a supervisor. I have learnt so much from him that I would continue to use both in my personal and professional lives. I will forever be indebted to him.

I am grateful to the administrative and research staff at the University of Adelaide. The staff and members of the Chapman Laboratory especially, were of immense help and working with them was a great pleasure.

My stay in Adelaide would not have been possible without the staff at the Kathleen Lumley College. I am particularly grateful to Ms Allyson Sandham for all her help.

I would also like to thank Dr. Andrei Kotousov for his invaluable inputs to my research and learning. I am also grateful to Dr. Abdul Sheikh for the numerous conversations and advice that he gave me while I was at the University of Adelaide.

I would like to thank the Westpac STEM Ph.D. program for the invaluable experience of working at a bank while doing my Ph.D.

I would also like to thank all my friends Tarun, Chandan, Parthan and Vivek for sticking with me through thick and thin.

Finally, words cannot describe the gratitude that I feel for my parents. It is rather futile trying to thank them, for I would not be here without them. They always put me at the centre of their lives and went through immense hardships to get me to where I am. I will continue to strive to make them happy.

I acknowledge that the research described in this thesis was financially supported by the Australian Research Council under grant number DE130100261. The support is greatly appreciated.

Table of Contents

List of Tables

List of Figures

Chapter 1

1. Introduction

Continuous monitoring the performance of structures in order to improve their safety and reliability is an issue of utmost importance in the areas of civil, aerospace and mechanical engineering. This concern has been the primary motivation for the development of Structural Health Monitoring (SHM) as a topic of research over the last few decades. The SHM of a structure is the process of detecting and evaluating the damage in a structure, with the help of embedded devices, such as actuators and sensors.

The discipline of SHM is also a result of evolution in the philosophy of design and maintenance of structures. From being driven by traditional design considerations and Fracture Mechanics in the early 1960s, evaluation and maintenance of structures has undergone a paradigm shift in the following decades. Development of maintenance procedures that could change from being ‘schedule-driven’ to ‘condition-based’, took precedence in the last three decades [1]. For this, it is necessary to develop systems that detect damage and evaluate the condition of a structure.

Damage can be defined as any structural or material change that compromises the safety and integrity of the structure. Some common examples of structural damage are corrosion, delamination and cracking. These damages are largely material and system dependent, and each of them is a specific topic of research. It is essential to understand the behaviour and properties of these damages to be able to detect them quickly. In addition to the above damages, with an increase in material science research, the number of new materials that are being used has seen a sharp rise. These materials often have unique and complex properties and newer kinds of structural damages that need to be further studied.

Empirical and qualitative methods have been used since as early as the 19th century, to test the functionality of structures. This was mainly due to the industrial revolution and an increased usage of metals for various purposes, such as manufacturing, transportation and infrastructure development. SHM, however, gained great prominence in early 1970s due to its necessity in the aerospace and offshore oil industries [2, 3]. These industries required real time damage detection and evaluation for the efficient maintenance of systems [2].

There are numerous methods in the field of SHM. These methods range from simple acoustic and ultrasonic methods to the more complicated ones such as radiography, magnetic fields, thermal fields and eddy-currents [4, 5]. However, one main drawback of methods such as ultrasound and eddy currents is that they are not well-suited for SHM due to integration or cost issues. These methods might prove particularly ineffective in large structures and structures with complex geometries. This is because there might be certain sections in the structure that are hard to access, leading to a possible omission of damage.

Another drawback, as noted by Doebling et al. [4], is that they require the probable location of damage to be known to the user beforehand.

Over time, some methods have been found to be more practical and viable for commercial use. The two most significant approaches that constitute the major fraction of research today in SHM are the Vibration based methods and the Guided Wave based testing methods.

1.1. Vibration based methods

Vibration based methods make use of the observation that changes to the material properties of a structure result in noticeable changes to the modal parameters of a structure. These changes in the material properties are generally classified as ‘damages’ and are of importance and interest to researchers. This could include the loss of material stiffness as in the case of fatigue damage, loss of isotropy as in the presence of a crack or the loss or gain of material that is observed in the case of corrosion.

The main drawback of vibration based methods is that they are costly when compared to the guided wave based methods. Rose [6] estimated guided wave based methods to cost less than 5% the cost of other damage detection methods. Low-frequency vibration based methods also lack the necessary sensitivity and resolution for quantitative evaluation of damage in materials, such as the fibre composite laminates. These materials are of great importance in the aerospace industry and require precise and sensitive techniques. They have been found to be better suited for certain guided wave based methods as discussed in the following section.

1.2. Guided wave based methods

SHM methods can be broadly classified into two categories: Active methods and Passive methods. Passive methods try to infer the presence and severity of the damage present, from the performance parameters of the structure. An example of a passive method, as suggested by Giurgiutiu [7], is trying to estimate the remaining service life of an aircraft from its operational parameters such as vibration levels, air speed, air turbulence etc. While these methods are useful in estimating the remaining functional life of a structure, they do not quantify the damage directly. Hence they might at best be conservative estimates of the health of a structure and at worst, grossly inaccurate.

Active methods, on the other hand, aim at directly evaluating the damage in a structure, guided wave based methods are active methods that evaluate the condition of the structure through the presence of embedded actuators and sensors. These sensors could range from conventional NDE transducers, that are difficult to be installed on a structure, to piezoelectric wafer thin sensors, that can easily be bonded to the surface of the structure [7].

Guided waves are stress waves forced to follow a path that is defined by the boundaries of the structure into which they are induced [1]. They are of special importance to SHM due to their unique property of travelling large distances with minimal dissipation. This allows them to traverse and inspect large areas for damage. Guided waves are also known to be well suited for curved and thin walled structures, which make them ideal for the testing of structures such as aircrafts, missiles, pressure vessels and oil tanks [7].

Some classes of guided waves that have been subject to research over the years are i) Rayleigh waves, which are surface-guided waves, travel near the surface of solids and have little penetration within the depth of the structure [1, 7, 8], ii) Stoneley waves that travel at the interface of two solid materials [1, 9], and iii) Lamb waves that travel in thin plate-like structures or shells. Lamb waves are of special interest to research in SHM due to the abundance of plate and shell structures, such as those in aircrafts and oil tanks.

Lamb waves were named after Horace Lamb who discovered the waves in 1917. However, it was Worlton [5], who first used them in damage detection in 1961 [10]. Prior to that, Mindlin and Schoch carried out considerable research in the field of Lamb waves in the early 1950s [10].

Lamb waves are also suitable for detecting internal damages in addition to surface damages owing to their ability to interrogate the entire plate thickness. They are not only very sensitive to the presence of damage, but can also detect multiple damages in the area of inspection [10]. Some of the other advantages of Lamb waves as discussed by Rose [6] are their ability to interrogate large areas from a single probe location, their cost advantage over the other methods and their ability to inspect insulated and coated surfaces including submerged structures.

Lamb waves, however, also have a few drawbacks, such as their ineffectiveness in anisotropic materials and presence of boundary-reflected waves in the wave-field [10]. The advantages nevertheless, far outweigh their drawbacks. Hence, the study of Lamb waves based methods has become the most significant topic of research among all other guided wave based methods.

A guided wave based method of great importance, that has taken precedence over the last decade and that is also a key topic of research for this project is the Lamb Wave Diffraction Tomography (LWDT) method. Tomography is the process of imaging a body by sectioning it into different planes. This process has long been used in the field of medicine where waves of shorter wavelength, such as X-Rays were used to derive an image of the visceral organs of the human body. This methodology is now used for reconstructing damage within structural components with the aid of Lamb waves that have a high sensitivity for structural damage.

One of the biggest advantages of LWDT over the other guided wave based methods is its cost effectiveness. Additionally, while techniques such as Artificial Intelligence methods are suitable for damage detection, they fail to reconstruct the geometry and physical characteristics of the damage, as efficiently as LWDT. LWDT is thus becoming one of the most commonly used SHM methods for both academic research and commercial use.

1.2.1. Lamb Wave Diffraction Tomography

LWDT is the process of interrogating a region of interest using pulsed Lamb waves and then gathering information about the damage in that region, from the scattered wave field. Various inverse analysis techniques have been developed to evaluate the damage from the scattered field. A strong understanding of the nature of damage and behaviour of Lamb waves is necessary for reconstructing the geometric or physical features of interest in the damage. LWDT is especially effective for corrosion damage, where there is a thickness reduction of the plate. It is also effective in identifying and evaluating delaminations within composite laminates.

Wang and Rose [11, 12] proposed a LWDT framework where the damage parameters were mathematically represented as local perturbations of the global material parameters. The scatter field amplitudes were then observed to be linearly related to the Fourier transform of these perturbation functions. Hence, the scattered field amplitude that was obtained either experimentally or computationally, was used to obtain the Fourier transform values of the perturbations which were in turn used to obtain the damage parameters through an inverse transformation. The framework was further investigated for corrosion damage in isotropic plates [10]. This approximation has a high degree of accuracy only for weak inhomogeneities. However, these weak inhomogeneities happen to be one of the major topics of research in SHM, as they correspond to early stage damage [12]. Developing algorithms to improve the efficiency of this framework, by incorporating a multi-frequency approach is of immediate importance in this field.

This thesis first examines and studies the phenomenon of mode conversion that is observed during the interaction of Lamb waves with a delamination. This gives us the knowledge that there is a whole set of information regarding multiple modes and frequencies, that can be tapped in order to increase the efficiency of the LWDT algorithm. We then move on to address the problem of incorporating multiple-frequencies into the LWDT framework so as to make the method more viable for commercial and research purposes. A multi-frequency approach greatly reduces the number of transducers that are required for image reconstruction, thus making the entire process easier to set up and implement.

1.3. Thesis structure

The contributions of this research are organised in the form of three journal publications. Chapters 2 and 3 are papers that have already been published with the same title as that of the chapters. Chapter 4 presents work that is currently under preparation. Chapter 5 presents the broad conclusions drawn from this thesis and the scope and direction of future work in this field. The following is a brief overview of the chapters.

Chapter 2: This chapter presents the scattering and mode conversion of anti-symmetric mode (A_0) Lamb waves in quasi-isotropic (QI) composite laminates. We observe the mode conversion from A_0 to the fundamental symmetric mode (S_0) Lamb wave (A_0-S_0) at the delamination. A three-dimensional (3D) explicit finite element (FE) model is proposed to simulate further results. An experimental study is also carried out to validate the results from the 3D FE model developed for the A_0 and S_0 Lamb wave propagation in composite laminates. This chapter studies the basic phenomenon of Lamb wave scattering at delaminations and gives us the information that multiple modes and consequently, multiple frequencies can be used to increase the efficiency of the LWDT algorithm.

Chapter 3: In this chapter, a series of numerical case studies are carried out for different sizes and shapes of damage. The image is reconstructed with multiple non-central frequencies to see if these frequencies can be used together to develop a multi-frequency algorithm for LWDT. The study shows that the non-central frequencies can indeed provide additional information for damage image reconstruction. Overall the results of the study in this chapter provide insights into

the influence of data at different frequencies, which is essential to advance the developments of LWDT.

Chapter 4: This chapter presents two algorithms that use multi-frequency data for the reconstruction of damage. Results are presented to show how a multi-frequency framework can significantly reduce the number of transducers used in order to develop an image of high resolution. These methods were tested for different damage shapes and locations to check their viability in different cases.

Chapter 5: The conclusions and inferences drawn from the work in this thesis are provided in this chapter. Probable scope and direction of future work in this field, is also addressed here.

1.4. List of Publications

The following is a list of the three journal publications and one conference paper that were produced from the work in this thesis.

1.4.1. List of Journal publications

1. Pudipeddi, G. T., Ng, C. T., & Kotousov, A. (2019). Mode Conversion and Scattering of Lamb Waves at Delaminations in Composite Laminates. *Journal of Aerospace Engineering, ASEC*, *32*(5), 04019067. **(Published)**
2. Pudipeddi, G.T., Ng, C.T. and Kotousov, A., 2018. Effect of central and non-central frequency components on the quality of damage imaging. *Journal of Civil Structural Health Monitoring*, *8*(1), pp.49-61. **(Published)**

3. Pudipeddi, G. T., Ng, C. T., & Kotousov, A. Multi-frequency methods for the reconstruction of damages in plate like structures. **(Under preparation)**

1.4.2. List of Conference publications

1. Pudipeddi GT, Ng CT (2017). 3D finite element prediction of scattering and mode conversion of Lamb wave at delaminations in composite laminates, *Structural Health Monitoring of Intelligent Infrastructure Conference* (SHMII-8), 5-8 December 2017, Brisbane, Australia

References

1. Raghavan A, Cesnik C.E..S. Review of Guided Wave Structural Health Monitoring, *The Shock and Vibration Digest* 2007;
2. Farrar, C.R. and Doebling, S.W. (1999). Damage detection II: field applications to large structures. In: Silva, J.M.M. and Maia, N.M.M. (eds.), Modal Analysis and Testing, Nato Science Series. Dordrecht, Netherlands: Kluwer Academic Publishers.
3. Carden P.E, Fanning P., Vibration based condition monitoring: A Review, *Structural Health Monitoring*, 2004
4. Doebling S.W, Farrar C.R, Prime M.B, A summary review of vibration based damage identification methods, 1998
5. Doherty, J. E., 1987, Nondestructive Evaluation, Chapter 12 in *Handbook on Experimental Mechanics*, A. S. Kobayashi Edt., Society for Experimental Mechanics, Inc.
6. J.L. Rose, A Baseline and Vision of Ultrasonic Guided Wave Inspection Potential, ASME. J. Pressure Vessel Technol., 2002
7. V. Giurgiutiu, Structural Health Monitoring with Piezoelectric Wafer Active Sensors, Academic Press, 2007
8. Rayleigh, J. W. S. (1887). On Waves Propagated Along the Plane Surface of An Elastic Solid, *Proceedings of the London Mathematical Society*, **17**: 4–11.
9. Stoneley, R. (1924). Elastic Waves at the Surface of Separation of Two Solids, *Proceedings of the Royal Society of London, Series A,* **106**: 416–428.

10. Su. Z, Ye. L, Lu. Y, Guided Lamb waves for identification of damage in composite structures: A review, *Journal of Sound and Vibration* 295 (2006) 753–780
11. Wang, C. H., & Rose, L. R. F. (2003, March). Plate-Wave Diffraction Tomography for Structural Health Monitoring. AIP Conference Proceedings, 657(1):1615-1622.
12. L.R.F. Rose, M. Veidt, C.H.Wang, Mindlin plate theory for damage detection: Source solutions, Acoustical Society of America, 2004

Chapter 2

2. Mode conversion and scattering of Lamb waves at delaminations in composite laminates

(Paper 1, Published)

Gnana Teja Pudipeddi

Graduate Student, School of Civil, Environmental and Mining Engineering, The University of Adelaide, Adelaide, South Australia, 5005, Australia.

Email: gnanateja.pudipeddi@adelaide.edu.au

Ching-Tai Ng

Associate Professor, School of Civil, Environmental and Mining Engineering, The University of Adelaide, Adelaide, South Australia, 5005, Australia

Email: alex.ng@adelaide.edu.au

Andrei Kotousov

Professor, School of Mechanical Engineering, The University of Adelaide, Adelaide, South Australia, 5005, Australia.

Email: andrei.kotousov@adelaide.edu.au

Publication:

Pudipeddi, G. T., Ng, C. T., & Kotousov, A. (2019). Mode Conversion and Scattering of Lamb Waves at Delaminations in Composite Laminates. *Journal of Aerospace Engineering, ASCE*, *32*(5), 04019067.

Statement of Authorship

Title of Paper	Mode conversion and scattering of Lamb waves at delaminations in composite laminates
Publication Status	☑ Published ☐ Accepted for Publication ☐ Submitted for Publication ☐ Unpublished and Unsubmitted work written in manuscript style
Publication Details	Pudipeddi, G. T., Ng, C. T., & Kotousov, A. (2019). Mode Conversion and Scattering of Lamb Waves at Delaminations in Composite Laminates. *Journal of Aerospace Engineering*, *32*(5), 04019067

Principal Author

Name of Principal Author (Candidate)	Gnana Teja Pudipeddi		
Contribution to the Paper	Performed literature review and researched the topic, set up and conducted experimental studies, developed numerical models and analysed results, prepared the manuscript		
Overall percentage (%)	80%		
Certification:	This paper reports on original research I conducted during the period of my Higher Degree by Research candidature and is not subject to any obligations or contractual agreements with a third party that would constrain its inclusion in this thesis. I am the primary author of this paper.		
Signature		Date	03/07/2019

Co-Author Contributions

By signing the Statement of Authorship, each author certifies that:

i. the candidate's stated contribution to the publication is accurate (as detailed above);

ii. permission is granted for the candidate in include the publication in the thesis; and

iii. the sum of all co-author contributions is equal to 100% less the candidate's stated contribution.

Name of Co-Author	Ching Tai-Ng		
Contribution to the Paper	Supervised development of work and reviewed and corrected draft of manuscript		
Signature		Date	11/7/2019

Name of Co-Author	Andrei Kotousov		
Contribution to the Paper	Supervised development of work and reviewed and corrected draft of manuscript		
Signature		Date	11/7/2019

Please cut and paste additional co-author panels here as required.

Abstract

This paper presents a study of Lamb wave scattering and mode conversion at a delamination in quasi-isotropic (QI) composite laminates. This study employs the fundamental anti-symmetric mode (A_0) Lamb wave as the incident wave and investigates the A_0 scattered and mode conversion from A_0 to the fundamental symmetric mode (S_0) Lamb wave (A_0-S_0) at the delamination. A three-dimensional (3D) explicit finite element (FE) model is proposed to predict the Lamb wave propagation, A_0 scattering wave and A_0-S_0 mode conversion wave at the delamination. An experimental study is also carried out to demonstrate that the 3D FE model is able to provide a reasonable prediction for the A_0 and S_0 Lamb wave propagation in the composite laminates. The results show that the amplitudes of the A_0 scattered and A_0-S_0 mode converted Lamb wave depend on the fibre orientation of the outer laminae, and the size and through-thickness location of the delamination. In summary the results of this study can further advance the delamination detection techniques using Lamb wave and provide physical insight into the scattering and mode conversion of Lamb wave at the delamination.

Keywords:

Lamb wave, scattering, mode conversion, finite element, composite laminate, delamination

2.1. Introduction

Fibre-reinforced composite laminates have been widely employed in different engineering fields, such as aerospace, civil and automobile industries, due to their light weight, corrosion resistance and high stiffness properties. The composite laminates are fabricated by assembling layers of fibrous composite materials. The flexural strength of the composite laminates highly depends on shear transfer between each lamina, and hence, the separation of adjacent laminae could significantly reduce its flexural strength. This kind of separation or slippage between the laminae is called delamination. Delaminations are invisible on the surface of the composite laminates, and hence, it is hard to be effectively detected.

The detection of delamination requires reliable non-destructive evaluation (NDE) techniques. In the last two decades, different NDE techniques were developed to detect the delamination in the composite laminates, for example, conventional ultrasonic [1, 2], thermography [3, 4], eddy current [5, 6], vibration based techniques [7, 8], guided wave techniques [9, 11] and nonlinear ultrasonic techniques [12, 13]. In particular, guided wave techniques have been widely recognised as one of the cost effective and reliable approaches.

2.2. Developments of damage detection using Lamb waves

Lamb waves are guided wave propagation in thin plates, such as composite laminates. It has been widely demonstrated that Lamb waves are sensitive to subsurface damage and can be used to inspect large area [14, 15]. The development of using Lamb waves in damage detection can be categorised into two groups, development of damage detection technique using Lamb waves and fundamental understanding of Lamb waves interaction with the damage. In the

last decade, different types of damage detection techniques using Lamb wave [10, 13, 16] were developed to detect damages in structures. At the same time, different studies were carried out to investigate the scattering characteristics of Lamb wave in different types of damages. The phenomena of Lamb wave scattering at different types of damage, such as through hole [17, 18], blind hole [19, 20] crack [21, 22] and corrosion [23] in isotropic plates were studied in detail.

2.3. Scattering analysis of damage in composite laminates

The research has also been extended to the composite laminates. Ramadas *et al*. [24] investigated the mode conversion effect when the incident fundamental anti-symmetric mode (A_0) Lamb wave interacts with the entrance of a symmetric delamination, by which the fundamental symmetric mode (S_0) Lamb wave is generated and travels within each of the sub-laminate at the delamination. Ramadas *et al*. [25] then extended their study to asymmetrically located delamination in the composite laminates. It was observed that, in the case of symmetrically located delaminations, the newly generated A_0-S_0 wave is confined to the sub-laminates. In the case of asymmetrically located delaminations, one is able to observe the mode converted S_0 wave in both the reflected side and the transmitted side of the composite laminate. This phenomenon was studied numerically on a 2D model and the results were compared with experimental results.

Ng and Veidt [26, 27]proposed a 3D FE model to predict the A_0 Lamb wave scattering at the delaminations in the composite laminates. Both numerical simulations and experimental measurements were used to investigate the

characteristics of A_0 Lamb wave scattering at the delaminations. Leckey *et al*. [28] proposed a 3D elastodynamic finite integration technique to investigate the guided wave propagation and scattering at the delamination in the composite laminate. Experiments using laser doppler vibrometer were also carried out in their study. Murat *et al*. [29] investigated the A_0 Lamb wave scattering at the delamination in the composite laminates. Both 3D FE simulations and experiments were carried in the study. Their study mainly focuses on the mixed-mode defects and impact damage. Gupta and Rajagopal [30] employed the FE simulation and experimental measurement to investigate the S_0 Lamb wave interaction at the delaminations in the composite laminates. However, there are limited studies focused on mode conversion effect of Lamb wave scattering at the delamination in the composite laminates. This study employs the 3D FE simulations to investigate the A_0 Lamb wave scattering and mode conversion at the delaminations in composite laminates. The effect of the delamination size and through-thickness location of the delamination is investigated in this study.

The paper is organized as follows. The 3D explicit FE model is first presented in the next section. It provides a detailed description of the FE modelling. The experimental setup and the results obtained are described and compared with the results calculated by the 3D FE model. After that a series of numerical case studies are presented, in which different sizes of delamination and through-thickness locations are considered. Finally, a conclusion is provided in the last section to summarize the work done in this paper.

2.4. Three-dimensional Explicit Finite Element Model

A 3D FE model is developed to simulate the Lamb wave propagation, A_0 scattering and mode conversion from A_0 to S_0 wave at the delaminations in a quasi-isotropic (QI) composite laminate. The commercial software, ABAQUS, was used to generate the geometry of the QI composite laminate and perform the meshing of the FE model. The size of the FE model for the QI composite laminate is 200×250mm^2. The QI composite laminate is assumed to be made by eight Epoxide EHM-32 unidirectional carbon/epoxy prepreg tapes with stacking sequence of $[-45/45/0/90]_S$ [31, 32]. The elastic properties of the Epoxide EHM-32 are shown in Table 2.1, and the density and fibre volume fraction is 1300kg/m^3 and 0.52, respectively. The thickness of each lamina is 0.2mm, and hence, the total thickness of the QI composite laminate is 1.6mm.

Table 2.1: Elastic properties of Epoxide EHM-32 prepare lamina

Young's moduli	E_{11}	111GPa
	E_{22}	7.16GPa
	E_{33}	7.16GPa
Shear moduli	G_{12}	3.52GPa
	G_{13}	3.52GPa
	G_{23}	2.2GPa
Poisson's ratios	ν_{12}	0.33
	ν_{13}	0.33
	ν_{23}	0.44

Absorbing layers by increasing damping (ALID) [33-35] are modelled at three edges of the QI composite laminate as shown in Figure 2.1. A PZT is modelled on the fourth. This edge will therefore not contain a damping layer. ALID contains different layers of elements with gradually varying damping to absorb the wave passing through these layers. The purpose of the ALID is to

avoid the wave reflected from the boundaries of the QI composite laminate. Therefore, the A_0 scattered wave and A_0-S_0 mode converted wave can be extracted while the size of the FE model can be minimised to reduce the computational cost. The width of the ALID is 50mm, which contains 25 layers and the width of each layer is 2mm. In this study, the mass-proportional damping is used to model the ALID. A high rate of varying damping value for the ALID would create stiff material layers and generate reflected wave. A low rate of damping value, on the other hand, would lead to incomplete absorption of the wave. In this study, the values of the mass-proportional damping (α) across the ALID are calculated by Rajagopal et al. [34] and Mohseni & Ng [35]

$$\alpha(x) = \alpha_{max} X(x)^P \tag{1}$$

where x is the location from the boundary between the QI composite lamination and ALID. P=3 and α_{max}=3×10^6 are used in this study. Taking into account the ALID, the total size of the FE model is 300×300mm^2.

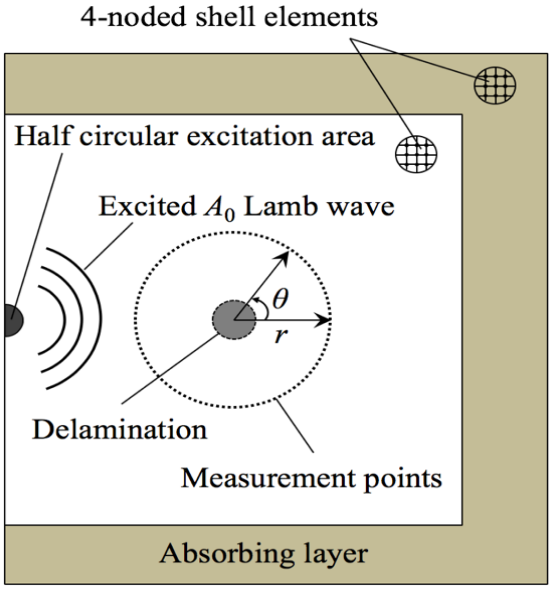

Figure 2.1: Schematic diagram of the 3D FE model

3D 4-node fully integration shell elements (S4) are used in this study. Each node of the shell elements has three translation degrees-of-freedom (DoFs) and three rotation DoFs. Two layers of shell elements are connected by tie constraint to model the QI composite laminate. The delamination is created by removing the tie constraint over the delamination area [36]. The thickness and number of laminae of the two layers of shell elements depend on the through-thickness location of the delamination. The size of shell elements used in the 3D FE model is around $0.5\times0.5mm^2$.

In this study, the A_0 Lamb wave is assumed to be excited by a 10mm diameter and 2mm thick half circular piezoceramic transducer. Based on the polar coordinator shown in Figure 2.1, the piezoceramic transducer is located at r = 125mm and $\theta = 180°$. The piezoceramic transducer is not modelled in the FE model, but the excitation is modelled by applying the out-of-plane nodal displacement to the nodal points covered by the assumed piezoceramic transducer. The excitation signal is 120kHz narrow-band five-cycle sinusoidal tone burst pulse modulated by a Hanning window. For calculating the A_0 scattered wave and A_0-S_0 mode converted wave, the out-of-plane and in-plane displacements were recorded at 36 nodal points, one for every 10^o at a constant distance from the centre of the damage. All explicit dynamic simulations were solved by ABAQUS/explicit. The time step was automatically controlled by ABAQUS/explicit.

2.5. Experimental Setup

An eight-ply QI composite laminate specimen was manufactured and the size of the specimen is $800\times800\times1.6mm^3$. The QI composite laminate was made by

Eporite EHM-32 unidirectional carbon/epoxy prepreg tapes and the stacking sequence is $[-45/45/0/90]_S$. The elastic properties are the same as in Table 2.1, and the fibre volume faction and stacking sequence are identical to the FE model described in the Section "Three-dimensional Explicit Finite Element Model".

A 10mm diameter and 2mm thick circular piezoceramic transducer was used to generate the A_0 incident Lamb wave. A 10mm diameter and 3mm thick circular brass was attached on the top of the piezoceramic transducer as a backing mass to increase the excitability of the A_0 Lamb wave. The centre of the piezoceramic transducer was bonded to the surface of the QI composite laminate using conductive epoxy and it is located at r = 125mm and $\theta = 180°$, which is identical to the FE model. Figure 2.2 shows a schematic diagram of the experimental setup. The excitation signal is a 10V peak-to-peak narrow-band five-cycle sinusoidal tone burst pulse modulated by a Hanning window. This excitation signal generated by a computer controlled arbitrary waveform generator is amplified by a power amplifier by a factor of 10-50 before it was sent to the piezoceramic transducer. A Polytec laser vibrometer was used to measure the Lamb wave signals. The measured data was then used to calculate the mode tuning curve, group velocity dispersion curve, directivity pattern of the incident wave, and the attenuation of the incident Lamb wave against the wave propagation distance.

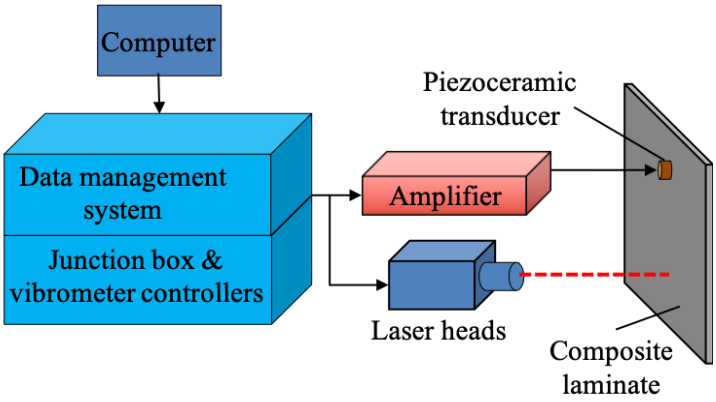

Figure 2.2: Schematic diagram of experiment setup

The excitation frequency was chosen to be 120kHz, which was decided based on the results obtained from the mode tuning analysis. The incident wave was generated by the piezoceramic transducer at frequency from 60kHz to 160kHz in steps of 10kHz, and the generated Lamb waves were measured at a fixed location away from the piezoceramic transducer using the laser vibrometer. At each excitation frequency, the amplitudes of S_0 and A_0 were recorded. Figure 2.3 shows the results of the mode tuning analysis. At 120kHz, the generated incident wave has a relatively high A_0 amplitude to S_0 amplitude ratio, and the measured signal has the minimum level of noise. Therefore, 120kHz was chosen in this study. The wavelength of A_0 Lamb wave at 120kHz is around 8.64mm.

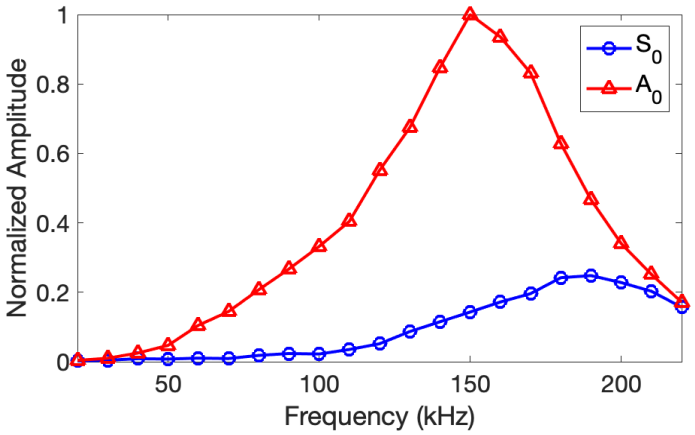

Figure 2.3: Mode tuning curve of a 2mm thick PZT with a 3 mm thick brass backing mass

2.5.1. Lamb wave propagation properties

A circular measurement configuration with 100mm radius and centre located at the piezoceramic transducer was used to measure the incident A_0 Lamb wave amplitudes at different directions at 120kHz. There are 36 measurement points in the circular measurement configuration and they are 10° away from each other. After the displacements were measured at these locations, the absolute amplitudes of the incident A_0 Lamb wave were extracted and the amplitude at each direction is normalised by the mean of the maximum absolute amplitudes of all directions. Figure 2.4 shows the experimentally measured and numerical results. The figure shows that the numerical results have reasonable agreement with the experimentally measured results.

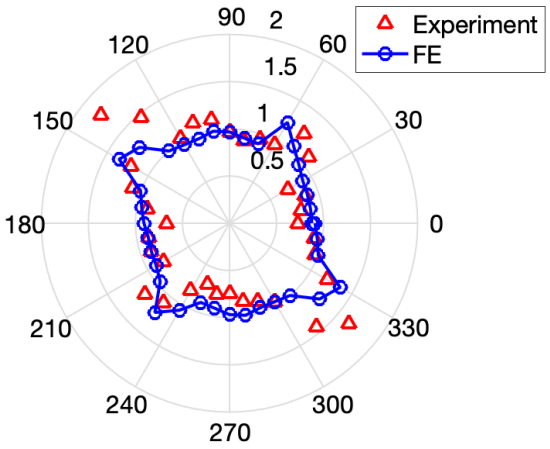

Figure 2.4: Normalized polar directivity pattern of the maximum absolute amplitude of the incident A_o wave at 120kHz in a $[-45/45/0/90]_S$ composite laminate

The attenuation property of the incident A_0 Lamb wave at 120kHz and in $\theta = 0°$ direction was experimentally measured and computationally simulated. The out-of-plane displacements were obtained from 20mm to 100mm away from the piezoceramic transducer and the step increment is 10mm. Figure 2.5 shows the experimentally measured and computationally simulated amplitude of the incident A_0 Lamb wave. The amplitude is normalized by the amplitude measured at 20mm away from the piezoceramic transducer. The results show that the attenuation property of the FE simulated A_0 Lamb wave has good agreement with the experimentally measured data.

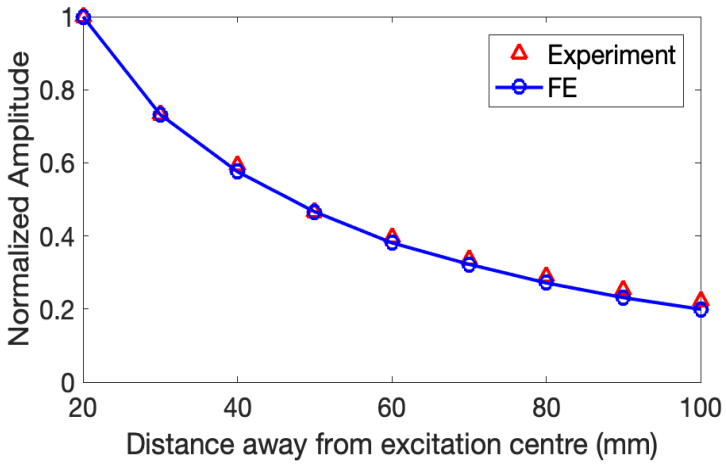

Figure 2.5: Normalized out-of-plane displacement amplitude as a function of wave propagation distance at $\theta = 0^{o}$ and 120kHz

Figure 2.6 shows that group velocity dispersion curve in $\theta = 0°$ direction. Both experimentally measured and computationally simulated group velocities are shown in the figure. The group velocity curve were obtained by sweeping the excitation frequency from 60kHz to 160kHz in steps of 20kHz. The group velocities calculated by DISPERSE software are also shown in Figure 2.6. The results show that the computationally simulated group velocities have good agreement with the theoretical and experimental results for both S_0 and A_0 Lamb wave. The results show that the 3D FE model is able to provide correct prediction for the S_0 and A_0 Lamb wave propagation.

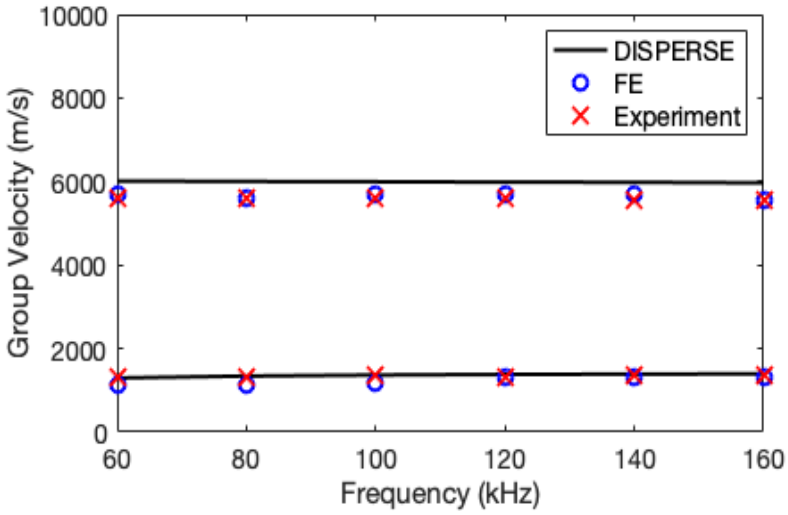

Figure 2.6: Group velocity dispersion curve at θ = 0°

2.6. Numerical case studies

The 3D FE model described in the Section "Three-dimensional Explicit Finite Element Model" is used to study the A_0 scattered and A_0-S_0 mode converted Lamb wave at the delaminations in a series of numerical case studies. The in-plane and out-of-plane nodal displacements at r = 80mm and 0°≤θ≤360° (as shown in Figure 2.1) with 10° step increment are calculated using the 3D FE model. In this study, the baseline subtraction approach is used to extract the A_0 scattered and A_0-S_0 mode converted Lamb wave. The baseline subtraction approach requires two simulations, intact model and model with the delamination, and the FE meshes of these two models are identical. The A_0 scattered and A_0-S_0 mode converted Lamb wave at the delamination can be calculated by

$$u_{r,\theta}^{(S)}(t) = u_{r,\theta}^{(D)}(t) - u_{r,\theta}^{(U)}(t) \tag{2}$$

$$v_{r,\theta}^{(S)}(t) = v_{r,\theta}^{(D)}(t) - v_{r,\theta}^{(U)}(t) \tag{3}$$

where the u and v are the in-plane and out-of-plane nodal displacement respectively. The superscripts (S), (D) and (U) means the scattered signal, and signal obtained from model with and without the delamination, respectively. $v_{r,\theta}^{(S)}$ is the A_0 scattered Lamb wave and $u_{r,\theta}^{(S)}$ is the A_0-S_0 mode converted Lamb wave. In this study, the amplitude of the A_0 scattered Lamb wave and A_0-S_0 mode converted Lamb wave are normalized as

$$\bar{u}_{r,\theta}^{(S)} = \frac{\left|u_{r,\theta}^{(S)}\right|}{max\left(\left|v_{0,\theta}^{(U)}\right|\right)} \tag{4}$$

$$\bar{v}_{r,\theta}^{(S)} = \frac{\left|v_{r,\theta}^{(S)}\right|}{max\left(\left|v_{0,\theta}^{(U)}\right|\right)} \tag{5}$$

where $v_{0,\theta}^{(U)}$ is the maximum out-of-plane displacement at the delamination centre location obtained from the model without the delamination.

2.6.1. A_0 scattered Lamb wave

This section investigates the A_0 Lamb wave scattering and A_0-S_0 mode conversion at different sizes of delaminations. The delaminations are all located between third and fourth lamina. The scattering directivity pattern (SDP) (Ng & Veidt 2011) of the A_0 scattered and A_0-S_0 mode converted Lamb wave are used to present the results. Figure 2.7 shows the SDP of the A_0 scattered wave at the delaminations. Figures 2.7a-d show the SDPs for the 7.5mm, 12.5mm, 17.5mm and 20mm diameter delaminations, respectively. The results show that the amplitude of A_0 scattered wave depends on the stacking sequence of the composite laminate. In this study, the fibre orientations at the outer laminae are -45° and 45° and the scattering wave energy focuses around these two directions. This phenomenon is consistent with the finding in Veidt and Ng (2011). For larger size of the

delamination, the energy of the A_0 scattered wave tends to be mainly focused in the forward directions.

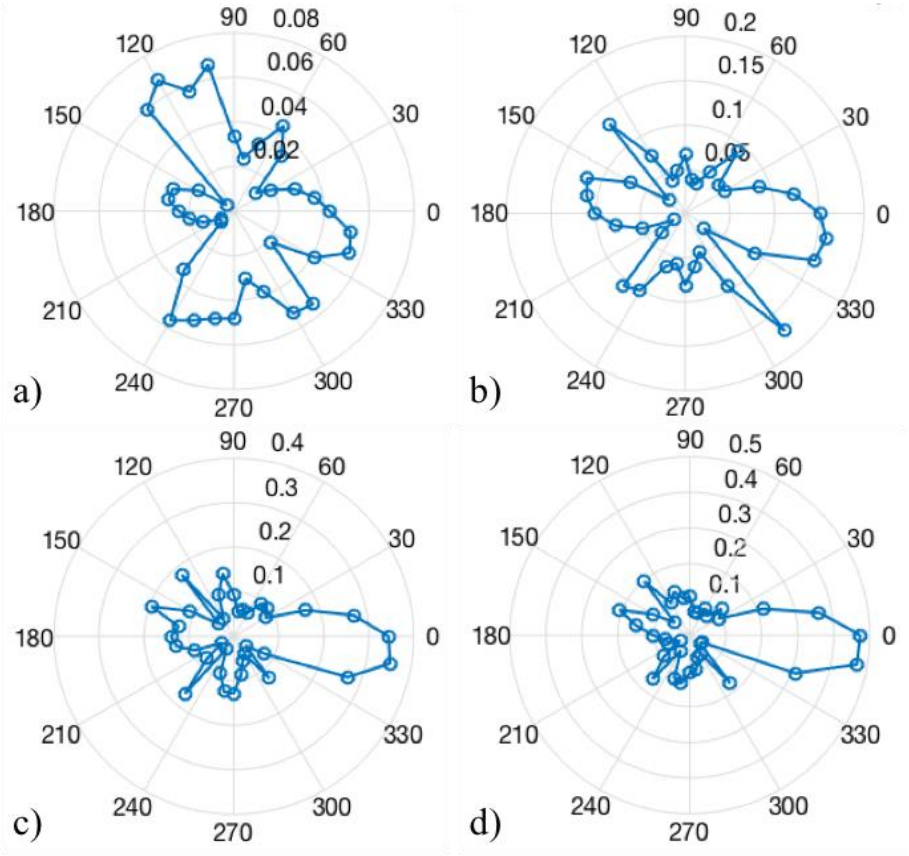

Figure 2.7: SDP of A_0 scattered wave for a) 7.5mm, b) 12.5mm, c) 17.5mm and d) 20mm diameter delamination located between 3rd and 4th lamina

2.6.2. A_0-S_0 mode converted Lamb wave

In addition to the A_0 scattered Lamb wave, the A_0-S_0 mode converted Lamb wave at these delaminations is also calculated and the results are shown in Figure 2.8. The SDP of the A_0-S_0 mode converted Lamb wave and the amplitudes are normalized using Equation (4). As shown in Figure 2.8, the amplitude of the A_0-S_0 mode converted wave is smaller than the A_0 scattered Lamb wave. This indicates when the A_0 Lamb wave interacts with the delamination, it produces A_0-S_0 mode converted Lamb wave, but the energy is small. The SDP shown in Figure

2.8 indicates that the A_0-S_0 mode converted Lamb wave is also influenced by the stacking sequence of the composite laminates. Similar to the A_0 scattered wave, the energy of the A_0-S_0 mode converted Lamb wave mainly focuses around fibre orientation of the outer laminae, i.e. at -45° and 45°. For larger size of delamination, the A_0-S_0 mode converted Lamb wave has larger amplitude.

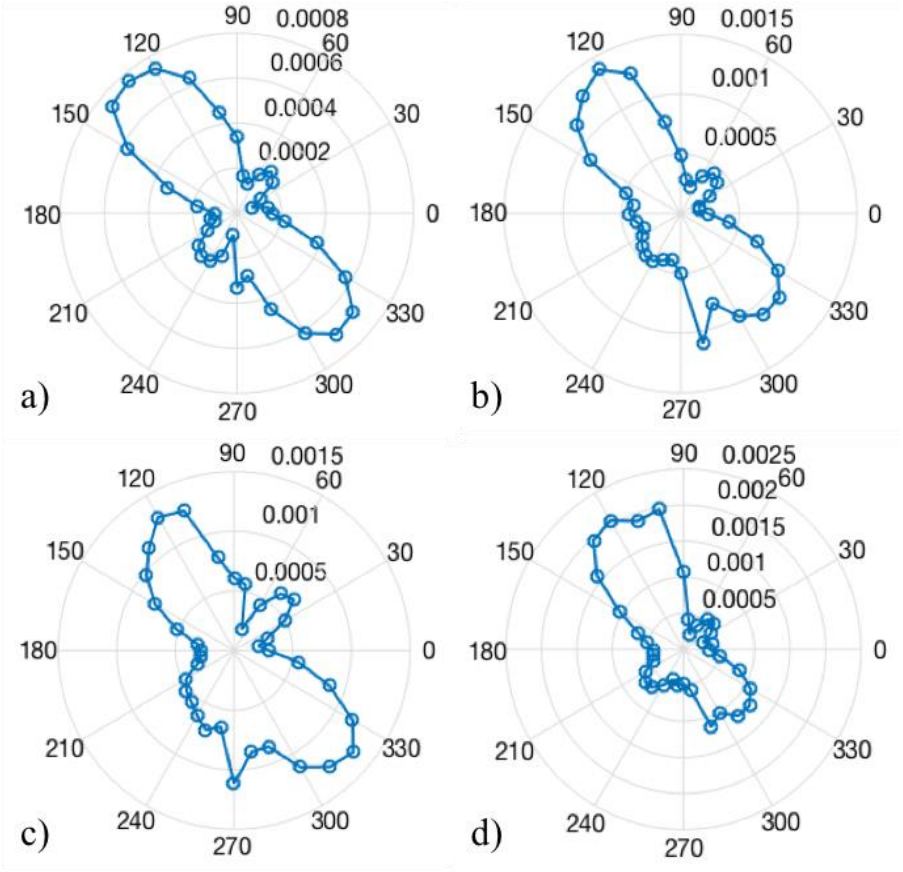

Figure 2.8: SDP of A_0-S_0 mode converted wave for a) 7.5mm, b) 12.5mm, c) 17.5mm and d) 20mm diameter delamination located between 3rd and 4th lamina

2.6.3. Effect of delamination size

A further investigation was carried to study the characteristics of the A_0 scattered and A_0-S_0 mode converted Lamb wave. Different sizes of delamination are considered in this study. Without loss of generality, the study is in terms of

delamination diameter to A_0 incident wave wavelength ratio (R_{DW}). The range of the R_{DW} considered is from 0.58 to 2.31, which covers seven sizes of delaminations. Figures 2.9a and 2.9b show the forward (θ = 0°, 20°, 40°, 320° and 340°) and backward (θ =140°, 160°, 180°, 200° and 220°) A_0 scattered Lamb wave. In general, the amplitudes of the A_0 scattered wave in forward direction are larger than backward direction, especially when the R_{DW} become larger. In the forward direction, for the A_0 scattered wave, the amplitudes increase linearly with R_{DW}. There is a small variation at some specific directions, i.e. θ = 180° and 200°, but trends of the amplitudes in the backward directions are in general increase with R_{DW}.

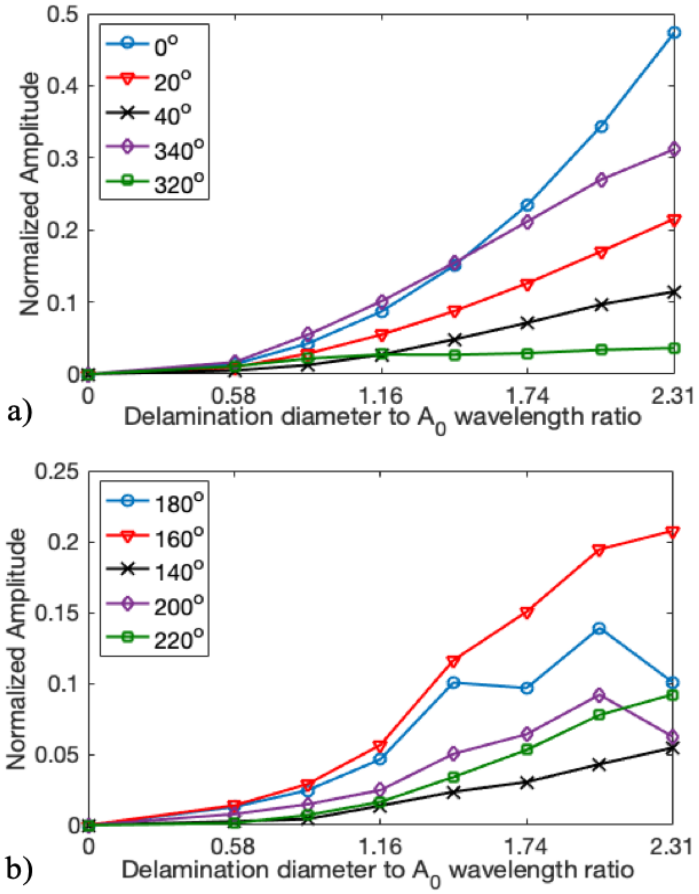

Figure 2.9: Normalized amplitude for the a) forward and b) backward A_0 scattered wave

Figures 2.10a and 2.10b show the corresponding forward and backward A_0-S_0 mode converted Lamb wave for different sizes of delaminations. The amplitude of A_0-S_0 mode converted Lamb wave is always smaller than the A_0 scattered Lamb wave. In general, the amplitude of the A_0-AS_0 mode converted Lamb wave has an increasing trend with small variation.

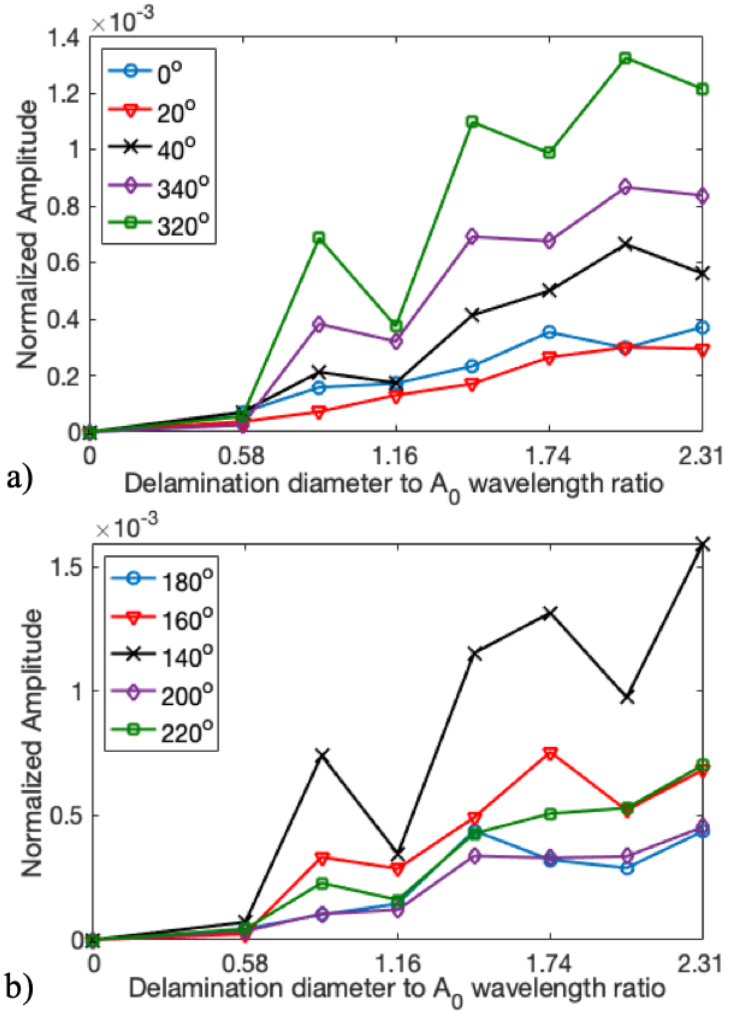

Figure 2.10: Normalized amplitude for the a) forward and b) backward A_0-S_0 mode converted Lamb wave

2.6.4. Effect of through-thickness location of delamination

In this section, the effect of through-thickness location of delamination is investigated. A fixed size of delamination (20mm diameter) is simulated at different through-thickness locations. The SDP of the A_0 scattered and A_0-S_0 mode converted Lamb wave are shown in Figures 2.11 and 2.12, respectively. Figures 2.11a, 2.11b and 2.11c show the SDP of A_0 scattered wave at delamination located between, first and second, second and third, and third and fourth layers, respectively. Since the 20mm diameter delamination is considered as a large damage, the energy of the A_0 scattered wave mainly focuses in the forward direction. Figures 2.12a, 2.12b and 2.12c show the corresponding SDP of the A_0-S_0 mode converted Lamb wave. The energy of the mode converted wave also depends on the fibre orientation of the outer laminae.

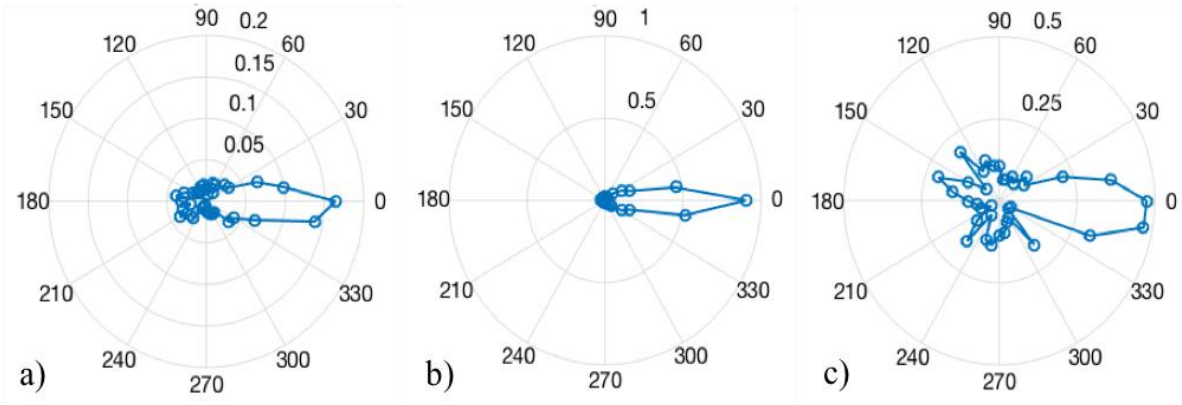

Figure 2.11: SDP of A_0 scattered wave for a 20mm diameter delamination located between a) 1st and 2nd, b) 2nd and 3rd, and c) 3rd and 4th lamina

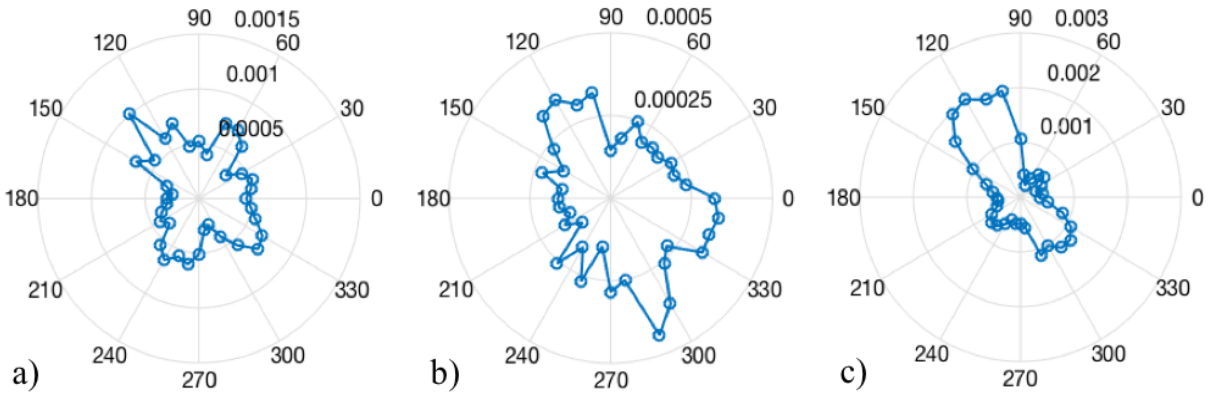

Figure 2.12: SDP of A_0-S_0 mode converted wave for a 20mm diameter delamination located between a) 1st and 2nd, b) 2nd and 3rd, and c) 3rd and 4th lamina

2.7. Conclusions

This paper has investigated the scattering and mode conversion of Lamb wave at the delaminations in the $[-45/45/0/90]_S$ QI composite laminate. The A_0 Lamb wave has been used as incident wave and the A_0 scattered and A_0-S_0 mode converted Lamb wave have been studied in details. A 3D FE model has been proposed to predict the wave propagation, scattering and mode conversion at the delamination. An experimental study has been carried out and the results have shown that the 3D FE model is able to provide a reasonable prediction of A_0 and S_0 Lamb wave propagation. A series of numerical case studies have been carried out to investigate the A_0 scattered and A_0-S_0 mode converted Lamb wave characteristics at the delamination using the 3D FE model. From the results of the SDPs, it has been shown that both A_0 scattered and A_0-S_0 mode converted Lamb wave are influenced by the fibre orientation of the outer laminae. In general, the amplitude A_0 scattered and A_0-S_0 mode converted Lamb wave have an increasing trend with the delamination size. Finally, the effect of the through-thickness

location of the delamination on the A_0 scattered and A_0-S_0 mode converted Lamb wave has also been demonstrated using the SDP. Overall, the findings of this study can provide improved physical insight into the scattering and mode conversion of Lamb wave at delamination. The results can help further develop the delamination detection techniques in the composite laminate.

References

1. Kazys, R. and Svilainis, L. 1997. “Ultrasonic detection and characterization of delaminations in thin composite plates using signal processing techniques.” *Ultrasonics* 35(5): 367-383.
2. Imielinska, K., Castaings, M., Wojtyra, R. Haras, J., Le Clezio, E. and Hosten, B. 2004. “Air-coupled ultrasonic C-scan technique in impact response testing of carbon fibre and hybrid: glass, carbon and Kevlar/epoxy composite laminates. *Journal of Materials Processing Technology*.” 157-158: 513-522.
3. Avdelidis, N.P., Hawtin, B.C. and Almond, D.P. 2003. “Transient thermography in the assessment of defects of aircraft composites.” *NDT&E International* 36(6): 433-439.
4. Sinha, A., Sastry, O.S. and Gupta, R. 2015. “Detection and characterisation of delamination in PV modules by active infrared thermography.” *Nondestructive Testing and Evaluation* 31(1): 1-16.
5. Mook, G., Lange, R. and Koeser, O. 2001. “Non-destructive characterisation of carbon-fibre-reinforced plastics by means of eddy-current.” *Composite Science and Technology* 61(6): 865-873.
6. Mizukami, K., Mizutani, Y., Todoroki, A. and Suzuki, Y. 2015. “Detection of delamination in thermoplastic CFRP welded zones using induction heating assisted eddy current testing.” *NDT&E International* 74: 106-111.
7. Zhang, Z., Zhan, C., Shankar, K., Morozov, E.V., Singh, H.K. and Ray, T. 2017. “Sensitivity analysis of inverse algorithms for damage detection in composite.” *Composite Structures* 176: 844-859.

8. Pan, J., Zhang, Z., Wu, J., Ramakrishnan, K.R. and Singh, H.K., 2019. A novel method of vibration modes selection for improving accuracy of frequency-based damage detection. *Composites Part B: Engineering*, *159*, pp.437-446.
9. Ng, C.T. 2015. "A two-stage approach for quantitative damage imaging in metallic plates using Lamb waves." *Earthquakes and Structures* 8(4): 821-841.
10. Ng, C.T. 2015. "On accuracy of analytical modelling of Lamb wave scattering at delaminations in multi-layered isotropic plates." *International Journal of Structural Stability and Dynamics* 15(8): 1540010.
11. He, S. and Ng, C.T. 2017. "Guided wave-based identification of multiple cracks in beams using a Bayesian approach." *Mechanical Systems and Signal Processing* 84: 324-345.
12. Solimanpour, R. and Ng, C.T. 2017. "Locating delaminations in laminated composite beams using nonlinear guided wave." *Engineering Structures* 131: 207-219.
13. Yang, Y., Ng, C.T., Kotousov, A., Sohn, H. and Lim, H.J. 2018. "Second harmonic generation at fatigue cracks by low-frequency Lamb waves: experimental and numerical studies." *Mechanical Systems and Signal Processing* 99: 760-773.
14. Kessler, S.S, Spearing, S.M. and Soutis, C. 2002. "Damage detection in composite materials using Lamb wave methods." *Smart Materials and Structures* 11: 269-278.

15. Diamanti, K. Hodgkinson, J.M. and Soutis, C. 2004. “Detection of low-velocity impact damage in composite plates using Lamb wave.” *Structural Health Monitoring* 3(1): 33-41.
16. Sherafat, M.H., Quaegebeur, N., Hubert, P., Lessard, L. and Masson, P. 2018. “Experimental model of impact damage for guided wave-based inspection of composites.” *ASME Journal of Nondestructive Evaluation* 1(4): 040801.
17. Diligent, O., Grahn, T. and Bostrom, A. 2002. “The low-frequency reflection and scattering of the S_0 Lamb mode from a circular through-thickness hole in a plate: finite element, analytical and experimental studies. *Journal of the Acoustical Society of America* 112: 2589-2601.
18. Fromme, P. and Sayir, M.B. 2002. “Measurement of the scattering of a Lamb wave by a through hole in plate,” *Journal of Acoustical Society of America* 111: 1165–1170.
19. Grahn, T. 2003. “Lamb wave scattering from a circular partly through-thickness hole in a plate.” *Wave Motion* 37(1): 63-80.
20. Cegla, F.B., Rohde, A., and Veidt, M. 2008. “Analytical prediction and experimental measurement for mode conversion and scattering of plate waves at non-symmetric circular blind holes in isotropic plates.” *Wave Motion* 45: 162-177.
21. Flores-Lopez, M.A. and Gregory, R.D. 2006. “Scattering of Rayleigh-Lamb waves by a surface breaking crack in an elastic plate. *Journal of Acoustical Society of America* 119: 2041-2049.
22. Ratassepp, M., Lowe, M.J.S., Cawley, P. and Klauson, A. 2008. “Scattering of the fundamental shear horizontal mode in a plate when incident at a

through crack aligned in the propagation direction of the mode." *Journal of Acoustical Society of America* 124: 2873-2882.

23. Moreau L., Velichko, A. and Wilcox, P.D. 2012. "Accurate finite element modelling of guided wave scattering from irregular defects." *NDT&E International* 45, 46–54.
24. Ramadas, C., Balasubramaniam, K., Joshi, M. and Krishnamurthy, CV. (2009), "Interaction of primary anti-symmetric Lamb mode with symmetric delaminations: numerical and experimental studies." *Smart Material and Structures* 18(8): 085011.
25. Ramadas, C., Balasubramaniam, K., Joshi. M. and Krishnamurthy. C.V. (2010), "Interaction of guided Lamb waves with an asymmetrically located delamination in a laminated composite plate." *Smart Material and Structures* 19(6): 065009.
26. Veidt, M. and Ng, C.T. 2011. "Influence of stacking sequence on scattering characteristics of the fundamental anti-symmetric Lamb wave at through holes in composite laminate." *Journal Acoustical Society of America* 129(3): 1280-1287.
27. Ng, C.T. 2011. "Scattering of the fundamental anti-symmetric Lamb wave at delaminations in composite laminates." *Journal of Acoustical Society of America* 129(3): 1288-1296.
28. Leckey, C.A.C., Rogge, M.D. and Parker, F.R. 2014. "Guided waves in anisotropic and quasi-isotropic aerospace composites: three-dimensional simulation and experiment. *Ultrasonics* 54(1): 385-394.

29. Murat, B.I.S., Khalili, P. and Fromme, P. 2016. “Scattering of guided waves at delaminations in composite plates.” *Journal of Acoustical Society of America* 139(6): 3044-3052.

30. Gupta, S. and Rajagopal, P. 2018. “Effect of ply orientation and through-thickness position of delamination on the reflection of fundamental symmetric S_0 Lamb mode in GFRP composite plate structures.” *Ultrasonics* 90: 109-119.

31. Ng, C.T., Pudipeddi, G.T. and Kotousov, A. 2017a. “3D finite element prediction of scattering and mode conversion of Lamb waves at delaminations in composite laminates.” *In Proc. 8th Int. Conf. on Structural Health Monitoring of Intelligent Infrastructure (SHMII-8),* Brisbane, Australia.

32. Ng, C.T., Pudipeddi, G.T. and Kotousov, A. 2017b. “Numerical simulation and experimental verification of Lamb wave scattering and model conversion at delaminations in composite laminates.” *In Proc. 9th Australasian Congress on Applied Mechanics (ACAM9)*: 533-539, Sydney, Australia.

33. Drozdz, M., Moreau, L., Castaings, M., Lowe, M.J.S. and Cawley, P. 2006. “Efficient numerical modelling of absorbing regions for boundaries of guided wave problems.” *AIP Conference Proceedings* 820(1): 126-133:

34. Rajagopal, P., Drozdz, M., Skelton, E.A., Lowe, M.J.S. and Craster, R.V. 2012. “On the use of absorbing layers to simulate the propagation of elastic waves in unbounded isotropic media using commercial available finite element packages.” *NDT&E International* 51: 30-40.

35. Mohseni, H., & Ng, C.-T. (2019). Rayleigh wave propagation and scattering characteristics at debondings in fibre-reinforced polymer-retrofitted concrete structures. *Structural Health Monitoring*, *18*(1), 303–317.

36. Mohseni, H. and Ng, C.T. 2018. "Higher harmonic generation of Rayleigh wave at debondings in FRP-retrofitted concrete structures." *Smart Materials and Structures* 27: 105038.

37. Yang, B., Xuan, F.Z., Chen, S., Zhou, S., Gao, Y. and Xiao, B. 2017. "Damage localization and identification in WGF/epoxy composite laminates by using Lamb waves: experiment and simulation." *Composite Structures* 165: 138-147.

Chapter 3

3. Effect of central and non-central frequency components on the quality of damage imaging

(Paper 2, Published)

Gnana Teja Pudipeddi

Graduate Student, School of Civil, Environmental and Mining Engineering, The University of Adelaide, Adelaide, South Australia, 5005, Australia.

Email: gnanateja.pudipeddi@adelaide.edu.au

Ching-Tai Ng

Associate Professor, School of Civil, Environmental and Mining Engineering, The University of Adelaide, Adelaide, South Australia, 5005, Australia (Corresponding author).

Email: alex.ng@adelaide.edu.au

Andrei Kotousov

Professor, School of Mechanical Engineering, The University of Adelaide, Adelaide, South Australia, 5005, Australia.

Email: andrei.kotousov@adelaide.edu.au

Publication:

Pudipeddi, G.T., Ng, C.T. and Kotousov, A., 2018. Effect of central and non-central frequency components on the quality of damage imaging. *Journal of Civil Structural Health Monitoring*, *8*(1), pp.49-61

Statement of Authorship

Title of Paper	Effect of central and non-central frequency components on the quality of damage imaging
Publication Status	☑ Published ☐ Accepted for Publication ☐ Submitted for Publication ☐ Unpublished and Unsubmitted work written in manuscript style
Publication Details	Pudipeddi, G.T., Ng, C.T. and Kotousov, A., 2018. Effect of central and non-central frequency components on the quality of damage imaging. *Journal of Civil Structural Health Monitoring*, *8*(1), pp.49-61.

Principal Author

Name of Principal Author (Candidate)	Gnana Teja Pudipeddi
Contribution to the Paper	Performed literature review and researched the topic, developed numerical models and studied various cases and frequencies, analysed and drew conclusions from the results, prepared the manuscript
Overall percentage (%)	80%
Certification:	This paper reports on original research I conducted during the period of my Higher Degree by Research candidature and is not subject to any obligations or contractual agreements with a third party that would constrain its inclusion in this thesis. I am the primary author of this paper.
Signature	Date: 03/07/2019

Co-Author Contributions

By signing the Statement of Authorship, each author certifies that:

i. the candidate's stated contribution to the publication is accurate (as detailed above);

ii. permission is granted for the candidate in include the publication in the thesis; and

iii. the sum of all co-author contributions is equal to 100% less the candidate's stated contribution.

Name of Co-Author	Ching Tai-Ng
Contribution to the Paper	Supervised development of work and reviewed and corrected draft of manuscript
Signature	Date: 11/7/2019

Name of Co-Author	Andrei Kotousov
Contribution to the Paper	Supervised development of work and reviewed and corrected draft of manuscript
Signature	Date: 11/7/2019

Please cut and paste additional co-author panels here as required.

Abstract

Accurate image reconstruction of damage through Lamb wave diffraction tomography (LWDT) requires substantial information of scatter field. This can be achieved by using a large number of transducers to collect the scatter field data. However, this requires an inordinate number of transducers that creates logistical constraints for the commercial applications of the technique. Various methods have been developed to improve the practicability of LWDT. One of the main approaches is to employ data at multiple frequencies within the bandwidth of the excitation signal. The objective of this study is to investigate the performance of using the data at non-central frequencies to reconstruct the damage image using LWDT. This provides an understanding on the influence of data at each individual frequency in the damage image reconstruction.

In this paper, a series of numerical case studies with consideration of different damage sizes and shapes are carried out. Different non-central frequencies data is used to reconstruct the damage image. The results show that using the data at different non-central frequencies leads to different qualities of the reconstructed damage images. The quality of these reconstructed damage images are then compared to investigate the information contained of the data at each individual frequency. The study shows that the non-central frequencies data can provide additional information in the damage image reconstruction using LWDT. Overall the results of this study provide insights into the influences of the data at different frequencies, which is essential to advance the developments of the LWDT.

Keywords:

Lamb wave, diffraction tomography, imaging, damage identification, structural health monitoring, scattering

3.1. Introduction

Structural health monitoring (SHM) has attracted increasing attention in the last two decades. It enhances reliability and sustainability of structures through providing in-situ structural monitoring. In the last decade, different damage detection techniques have been developed to provide early detection of damage and reduce the life-cycle costs of the structures. Early developments focused on non-destructive evaluation (NDE) techniques, such as visual inspection [1,2], conventional ultrasonic [3,4] and eddy-current techniques [5,6]. However, safety inspections using these techniques are usually carried during scheduled maintenance and they are not able to inspect inaccessible locations of the structures, as they need to be operated manually by experienced inspectors. In addition the coverage area is usually small in each inspection process. Therefore, the safety inspections using these NDE techniques are time-consuming and cost ineffective, and they are generally not suitable for SHM purposes. It is important to develop a reliable and robust damage detection that can provide in-situ monitoring of the structure. Guided wave based damage detection techniques are feasible for SHM as they are able to provide in-situ monitoring of structures. Additionally, they are sensitive to small and different types of damages, able to inspect inaccessible locations, and cost effective. These advantages make them to be one of the most promising damage detection methods.

3.2. Damage detection using Lamb wave

Lamb waves are mechanical stress wave that propagates along plate-like structures and are guided by structural boundaries. It is a type of guided wave. In the last two decades, Lamb waves have attracted considerable attention [7-11] in

SHM. To date, numerous damage detection techniques using Lamb waves have been developed, for example, time-of-flight approach [5], maximum-likelihood estimation [6], damage imaging [14-**Error! Reference source not found.**], phase rray approach [8], model based approach [18,19], time-reversal approach [20] and diffraction tomography [21-23]. Each of these techniques provides different levels of assessment of damages in the structures. While some methods are only able to determine the existence and location of the damages, some others provide more information, such as severity and shape of the damages.

Recently, developments have been extended to the concept of using the nonlinear guided wave for damage detection [24-28]. This is potential to address some bottlenecks of the linear guided wave approaches, e.g. the need of baseline data, which can be changed under varying temperature and operational conditions [29-31]. This study will only focus on the topic of linear guided wave and diffraction tomography approach. Therefore, the rest of this paper will focus on linear guided wave.

3.2.1. Lamb wave diffraction tomography

Apart from the essential requirements that the damage detection must be reliable and sensitive to the damages, two additional features: graphical representation and quantitative identification; can provide invaluable information for SHM. The former provides physical information for engineers in understanding the damage detection results and the latter provides comprehensive information, which can assist decision-making on the remedial work.

Lamb wave diffraction tomography (LWDT) is a quantitative damage detection technique that provides an efficient and cost effective inspection of a large area of structures. It utilizes the scattering effects of Lamb waves and

various tomographic algorithms to reconstruct robust images of the damages. The scattered wave field can be obtained by sequentially interrogating an area of interest with Lamb waves using multiple transducers. Early developments of tomographic imaging are based on the time-of-flight information of Lamb waves [32-34] to reconstruct an image of the damage. But this approach assumes that Lamb wave propagation is in the form of straight rays.

Malyarenko and Hinders [21] proposed a diffraction tomography approach that takes into account the diffraction effect of Lamb waves to improve the reconstructed image quality and resolution. Wang and Rose [22, 35] proposed a LWDT framework based on the Mindlin plate theory and Born approximation, which relates the scattered plate waves to the damage geometry. The damage parameters were mathematically represented as local perturbations of the global material parameters. The scatter field amplitudes were then found to have a linear relationship with the Fourier transform of these perturbation functions. Hence, once the Fourier transform values of the perturbations were obtained from the scattered field amplitudes, an inverse transformation could be applied to obtain the damage parameters. The framework was further investigated for corrosion damage in isotropic plates [10].

Belanger et al. [18] also proposed a LWDT framework based on the Born approximation. The framework examines the dependence of the phase velocity of the waves, on the plate thickness. The phase velocity of the fundamental anti-symmetric (A_0) mode of a Lamb wave is proportional to the square root of the frequency-thickness product. This implies that for constant frequency, Lamb waves have a lower velocity in the plate regions with reduced plate thickness. Hence, a diagnostic image of the damage can be reconstructed using the wave

velocity profile. After that various inverse methods and scattering models were also developed [38,39] to improve damage resolution and the computational efficiency of LWDT.

Development of accurate and simple inverse transformation techniques that do not require a large number of transducers for LWDT is a very important topic of research. In addition to the inverse Fourier transformation approach that was originally used for early development of LWDT, Devaney and Dennison [40] proposed a least-squares estimation method for inverse transformation. The least-squares estimation method was implemented by Rohde et al. [41] using a constrained linear inversion technique and the results were found to be more accurate and have better performance than the direct Fourier inversions approach.

One of the major requirements of the technique proposed by Wang and Rose is the assumption that the scatter field data collected is under far-field conditions [22,35,37]. That is, the distance between the sensors and the damage is greater than $2d^2/\lambda$, where d is the diameter of the damage and λ is the wavelength of the Lamb wave. However, a near-field imaging method is more practical as the damage may be closer to the transducer in real life applications. This drawback was addressed by Chan et al. [44] where they employed finite element based numerical Green's functions and the multi-static data matrix to overcome this constraint. The Green's functions can be defined as an undamaged structure's response to a unit input. They also showed that the numerical method suggested for the calculation of Green's functions is in agreement with the analytical function [35]. A similar numerical method, which significantly reduces the mathematical intensity of the solution, was also developed for the evaluation of the multi-static data matrix. They proposed that the Green's function can be

estimated by the ratio of the Fourier transforms of the response and the input forces at the central frequency.

In general the excitation signal for a Lamb wave is a narrowband signal, which contains multiple frequency components. While the central frequency of this signal is predominant and has the maximum amplitude in the Fourier transform of the signal, it can also be observed that the wave-field also contains a significant number of frequency components adjacent to the central frequency. A multi-frequency approach that incorporates the effects of the non-central frequencies in damage image reconstruction was proposed by Belanger et al. [36]. However, the effect of the non-central frequency components on the quality of the reconstruction damage imaging has not yet been examined. The aim of this paper is to examine the quality of the reconstructed damage image using LWDT based on the Mindlin plate theory and Born approximation when the non-central frequency components of response signals are used in the image reconstruction. This study will compare the quality of the reconstructed damage images using central and non-central frequency data of the measured signals. This provides an examination of the quality of the reconstructed damage image using LWDT when the non-central frequency components of response signals are used in the image reconstruction.

The paper is structured as follows: Section 2 describes the methodology of the near-field imaging algorithm. Section 3 presents the FE model in the numerical simulations and describes the details of the numerical case studies. The results and discussions can be found in Section 4. Finally, conclusions are drawn in Section 5.

3.3. Methodology

The LWDT requires a network of transducers to sequentially scan the plate, in which the transducers are used to transmit and receive Lamb wave signals. Using a pair of transducers as an example, Fig. 3.1 shows a schematic diagram of Lamb waves generated by a source transducer X_s, scattering at the damage region Σ_d, and then measured by the receiver transducer X_r. For a transducer network with N number of transducers, a number of the scattered wave signals can be collected from the sequential scan. The scattered wave signals are then used to reconstruct the damage using LWDT.

In this paper, the imaging algorithm used to reconstruct the damage is a near field imaging algorithm developed by Chan et el. [44]. This method was developed by extending the previously developed far-field imaging algorithm [22,35] to take into account the near field effect. In this section we first describe the far-field imaging algorithm developed by Rose and Wang [22,35] and then presents the near-field algorithm [44].

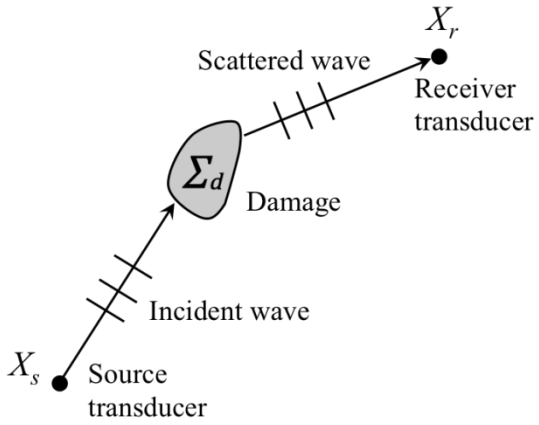

Figure 3.1: A schematic diagram of Lamb wave generation and scattering at damage

The far-field imaging algorithm with Born approximation [22] is appropriate for weak inhomogeneities in a plate. The Born approximation consists of approximating the total displacement with the incident wave displacement. The measured total displacement $\hat{w}$ is given by the expression:

$$\hat{w} = \hat{w}^I + \hat{w}^S \tag{1}$$

where $\hat{w}^I$ is the incident wave displacement and $\hat{w}^S$ is the scattered wave displacement. The "$\hat{}$" symbol means the frequency domain response obtained by the Fourier transform of the time-domain signal. Using the Born approximation, Eq. 1 becomes

$$\hat{w} = \hat{w}^I \tag{2}$$

The integral solution for a scattered field due to a defect can be represented by [22]:

$$\hat{w}^S(x,\omega) = \int\int k_1^2\, s(\xi)\hat{w}(x,\omega)G(x,\xi,\omega)d^2\xi \tag{3}$$

where k_1 denotes the wave number of the first flexural wave mode. $G(x,\xi,\omega)$ denotes the Green's function [35] of the scattered wave field from point ξ within the damage region Σ_d to point x on the plate. ω is the angular frequency. $s(\xi)$ is the damage potential that takes various physical forms depending on the nature of damage. In this case, $s(\xi)$ is the reduced thickness within the damage boundary

on the plate. Using the Born approximation, the total wave-field on the right-hand side of Eq. 3 can be replaced by the incident wave-field as

$$\widehat{w}^S(x,\omega) = \int\int k_1^2\, s(\xi)\widehat{w}^I(x,\omega)G(x,\xi,\omega)d^2\xi \tag{4}$$

Under far-field condition, the incident wave-field at ξ is given by:

$$\widehat{w}^I(x,\omega) = e^{i\boldsymbol{k_1}^I\xi} \tag{5}$$

and the Green's function [35] is given by

$$G(x,\xi;\omega) = \frac{i}{4}\sqrt{\frac{2}{\pi k_1 r}}\, e^{i\left(k_1 r - \pi/4\right)}\, e^{-k_1{}^S\xi} \tag{6}$$

where $k_1 r \rightarrow \infty$

where $\boldsymbol{k}_1^I = k_1\alpha = k_1(cos\alpha, sin\alpha)$ is the incident wave vector. Inserting Eqs. 6 and 5 into Eq. 4, the integral representation for the scattered field becomes

$$\widehat{w}^S(x,\omega) = \sqrt{\frac{i}{8\pi k_1 r}}\, e^{ik_1 r} A(\boldsymbol{k}_1^S, \boldsymbol{k}_1^I) \tag{7}$$

where $\boldsymbol{k}_1^S = k_1\theta = k_1(cos\theta, sin\theta)$ is the scattered wave vector. The physical significance of the Eq. 7 is the assumption that the damage is located at a distance

from the PZTs, where the incident wave amplitude can be described by the plane-wave scattering amplitude.

$$A(\theta, \alpha; 0) = \lim_{k_1 r \to \infty} \frac{\hat{w}^S(r,\theta;\omega)}{\sqrt{\frac{2}{\pi k_1 r}} e^{ik_1 r} e^{-i\pi/4}} \tag{8}$$

where $\hat{w}^S(r, \theta; \omega)$ is the scattered wave field along direction θ due to an incident plane-wave of unit strength in the direction α.

The fundamental concept of LWDT is to relate the two-dimensional (2D) spatial Fourier Transform of the inhomogeneity variation to the plane-wave scattering amplitude. The inhomogeneity variation is eventually reconstructed by taking an Inverse Fourier transformation in the wavenumber space [19]. For plate-wave case, this inversion in the ***k***-space is formulated as integrals over the source and receiver angles:

$$s(x) = \frac{1}{8\pi^2} \int_0^{2\pi} \int_0^{2\pi} \frac{A(\theta,\alpha;0)}{q_h(\theta-\alpha)} |\sin(\theta - \alpha)| e^{ik_1(\theta-\alpha)x} d\theta d\alpha \tag{9}$$

where $s(x)$ denotes the reconstructed value of the plate thickness reduction δh. The term $|sin\ (\theta - \alpha)|$ is the Jacobian for the change in integration variables from $(k_x^S - k_x^I, k_y^S - k_y^I)$ to (θ, α). The parameter $q_h(\theta - \alpha)$ is a function of the type of damage chosen, which is plate thickness reduction in this case. It denotes the shape function characterising the scattering pattern for a point-scatterer and is given by the following expressions [19]. For a damage that is characterized by plate thickness reduction,

$$q_h = 3q_1 + q_2 + 3q_3 + q_4 \tag{10}$$

where

$$q_1(\Delta\theta) = \frac{\gamma_1 {k_1}^2}{({k_1}^2 - {k_2}^2)}[cos^2\Delta\theta + \nu\, sin^2\Delta\theta] \tag{11}$$

$$q_2(\Delta\theta) = \frac{\bar{\mu}h(1-\gamma_1)^2}{\gamma_1 D({k_1}^2 - {k_2}^2)}[\cos\Delta\theta] \tag{12}$$

$$q_3(\Delta\theta) = -\frac{\gamma_1 \rho I \omega^2}{D({k_1}^2 - {k_2}^2)}[\cos\Delta\theta] \tag{13}$$

$$q_4(\Delta\theta) = -\frac{h\rho\omega^2}{\gamma_1 D {k_1}^2({k_1}^2 - {k_2}^2)} \tag{14}$$

where $\Delta\theta = \theta - \alpha$, or $\Delta\theta = \varphi_i - \varphi_j + \pi$ for the near field imaging formula, D denotes the bending stiffness of the plate, γ_1 is the wave amplitude ratio between the first and second branches of the wave mode. $k_{1,2}$ is the travelling and non-propagating wavenumber. $\bar{\mu}$ is the modified shear modulus. h is the plate thickness. ρ is the density of the plate material. ν is the Poisson ratio and I is the area moment of the vertical cross-section of the plate.

The near field algorithm [44] involves two major steps: i) the incident wave is expressed as a function of the vertical input force, ii) The plane wave scattering amplitude is expressed relative to the imaging point as opposed to the origin. When a vertical input force $\hat{F}(\omega)$ is applied by a transducer at location X_s = (x_s,

y_s), the incident wave generated by the transducer takes the following form as a function of its location x.

$$\widehat{w}^I(x,\omega;X_s) = \hat{F}(\omega)G(x,\omega;X_s) \tag{15}$$

where $G(x,\omega;X_s)$ denotes the plate–wave dynamic Green's function. Fig. 3.2 shows a schematic diagram of a PZT network and imaging domain for the LWDT. Using Eq. 8, the scattered field at a receiving transducer location $X_r = (x_r, y_r)$ can be expressed as

$$\widehat{w}^S(x_r, y_r;\ \omega) =$$

$$A\left(\varphi_{r,}\ \varphi_{s,} - \ \pi; x\right)\widehat{w}^I(x,\omega;X_s)\left(\frac{i}{4}\sqrt{\frac{2}{\pi k_1 r}}e^{ik_1\rho_r}e^{-i\pi/4}\right) \tag{16}$$

where $\widehat{w}^I$ is the incident wave given by Eq. 15 and ρ_r is the distance between a receiving sensor X_r and an imaging point x within the imaging domain. φ_r and φ_s are the receiver and source angles relative to the origin at the imaging point x as shown in Fig. 3.2. It can also be shown that the scattering amplitude relative to the origin at x can be related to the scattering amplitude relative to an origin at 0 by the following translation

$$A(\theta,\alpha;x) = A(\theta,\alpha;0)e^{ik_1(\theta-\alpha)x} \tag{17}$$

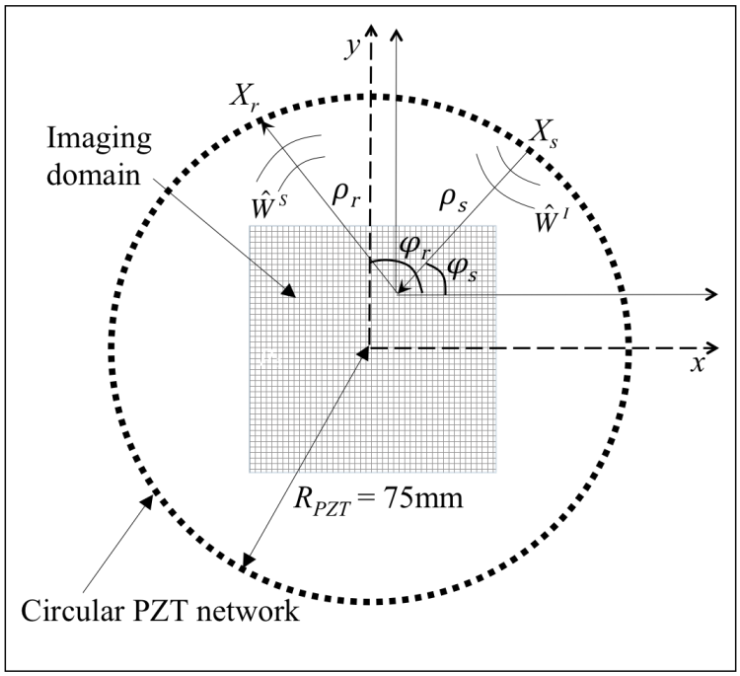

Figure 3.2: A schematic diagram of the PZT configuration and imaging domain for Lamb wave diffraction tomography

In this paper, we only consider an analytical value for the Green's function [35] as opposed to the Green's function obtained from numerical method [44]. It has been shown that for flat plate, the Green's functions obtained using numerical methods are similar to the Green's functions obtained from the analytical method [44]. This analytical Green's function is given by [35]:

$$G(X_r, \omega; x) = \frac{1}{D({k_1}^2 - {k_2}^2)\gamma_1} \frac{i}{4} \sqrt{\frac{2}{\pi k_1 r}} e^{ik_1\rho_r} e^{-i\frac{\pi}{4}} \tag{18}$$

Using Eq. 17 and 18, Eq. 9 can be rewritten in the following form:

$$s(x) = \frac{1}{8\pi^2 D\gamma_1({k_1}^2 - {k_2}^2)} \int_0^{2\pi} \int_0^{2\pi} \frac{K_{rs}|\sin(\varphi_r - \varphi_s)|}{G(X_r,x)G(x,X_s)q_h(\varphi_r - \varphi_s + \pi)} d\varphi_r d\varphi_s \tag{19}$$

where

$$K_{rs} = \frac{\hat{w}^S(X_r,\omega;X_s)}{\hat{F}(\omega)} \tag{20}$$

represents the scattered field data normalized relative to the amplitude of the actuating force at the central frequency of the input tone-burst.

The inversion integral in Eq. 19 can be evaluated as a discrete sum of values using the trapezoidal quadrature rule. This is due to the finite number of source and receiver transducers that are used for generating the scattered field. Thus Eq. 19 can be expressed as:

$$s(x) = Re\left[\frac{1}{8\pi^2 D\gamma_1\left({k_1}^2-{k_2}^2\right)}\sum_{j=1}^{N}\sum_{i=1}^{N}\frac{K_{ij}\left|\sin(\varphi_i-\varphi_j)\right|}{G(X_i,x)G(x,X_j)q_h(\varphi_i-\varphi_j+\pi)}\Delta\varphi_i\Delta\varphi_j\right] \tag{21}$$

where $\Delta\varphi_i = (\varphi_{i+1} - \varphi_{i-1})/2$ in which $\varphi_0 = \varphi_N - 2\pi$. K_{ij} is the multi-static matrix defined by Eq. 20. φ is the polar angle relative to the imaging point *x* as origin. Subscripts *i* and *j* are used to identify receiver and source locations, respectively. *N* is the total number of source and receiver sensors. The value of the thickness reduction in the damage is thus obtained using Eq. 21.

This paper aims to address the importance and efficacy of non-central frequencies in the development of image reconstruction algorithms. These frequencies have a two-fold advantage in the advancement of the Diffraction Tomography algorithm. Firstly, they reduce the number of PZTs and consequently the implementation costs, by using data from multiple frequencies. Secondly, they also improve the damage resolution by gathering additional data from the same number of PZTs as

before, thus giving a better image definition. Hence the objective is to only highlight their uniqueness and additional benefits but not to incorporate them into a new algorithm. This is achieved by examining the quality of the reconstructed damage image when the data at non-central frequencies is used to calculate the multi-static data matrix. This is carried out by taking the Fourier transform of the scattered field and extract the results at frequency that is $\pm N_f$ kHz away from the central frequency as shown in Fig. 3.3. It should be noted that care must also be taken in determining the corresponding value from the Fourier transform of the excitation force. In the next section the numerical case studies will be described in details, in which the effect of the data at each non-central frequency on the quality of the reconstructed damage image will be investigated.

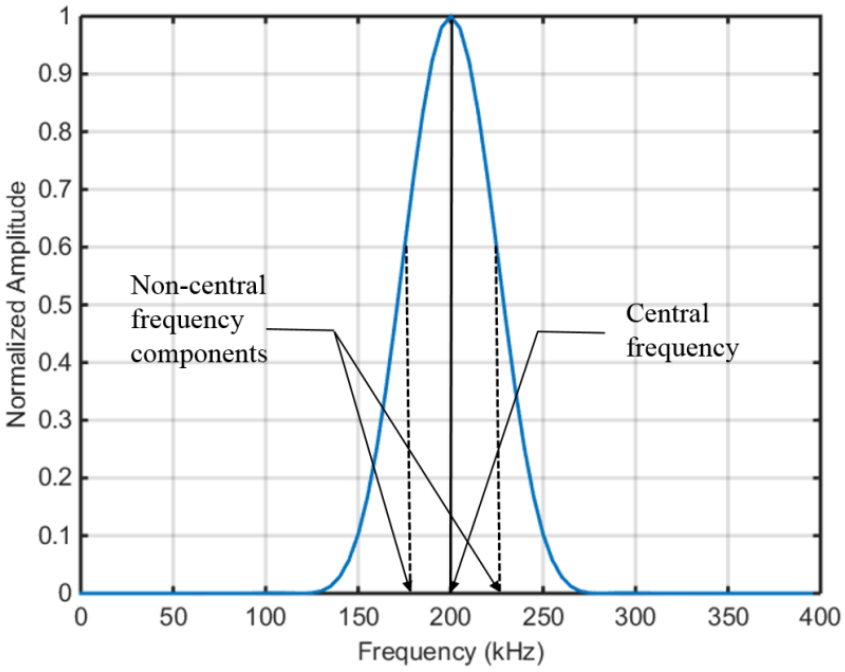

Figure 3.3: Central and non-central frequency components for a Lamb wave signal at 200 kHz (Solid line indicates central frequency and dashed lines indicate non-central frequencies)

3.4. Numerical Case Studies

The imaging algorithm is demonstrated using a numerical simulation model of an isotropic aluminium plate. The three-dimensional (3D) explicit finite element (FE) method [42,43] is used to simulate Lamb wave scattering phenomenon at damage in an aluminium plate. A commercial FE software, ABAQUS, was used to carry out the FE simulations in this study. The size of the plate is 240 mm × 240 mm and the thickness is 1.6 mm. The Young's modulus is 69 GPa, density is 2760 kg/m^3 and Poisson's ratio $\nu = 0.33$. The plate is modelled by eight-noded 3D reduced integration solid brick element (C3D8I) with incompatible modes. Each node of the solid brick element has three degrees-of-freedom (DoFs).

The fundamental anti-symmetric (A_0) Lamb wave is used as the incident wave and it is generated by transducers installed at the surface of the plate. In this study, only the deformations induced by the transducers are modelled, which is simulated by applying the out-of-plane nodal displacement at the required points. The excitation signal is a 200 kHz narrow-band five-cycle sinusoidal tone burst pulse modulated by a Hanning window. While any frequency that does not lead to the generation of higher mode Lamb waves is acceptable for the simulation, a frequency of 200 kHz was chosen so as to generate a wave with a wavelength that is comparable to the size of the damage taken. The wavelength of the generated A_0 Lamb wave is 7.5 mm. Lower frequencies also ensure a pronounced A_0 mode relative to the S_0 mode. A circular transducer network, which contains 128 transducers, is used to actuate and measure the Lamb wave signals in this study. The radius of the circular transducer network is $10\lambda = 75$ mm. The Lamb wave

signals at particular locations are obtained by calculating the out-of-plane nodal displacement of the nodes located at the surface of the plate.

In the FE model, most of the solid brick elements have an in-plane square shape with dimensions 0.4×0.4 mm^2. This means that there are at least 12 nodes per wavelength and five layers of FE element in the thickness direction to ensure the accuracy of the Lamb wave simulation results. The model has six layers of elements along its thickness with the top and bottom layers having a height of 0.08 mm. The other four layers in between are of thickness 0.36 mm. The incremental time step of the explicit FE simulation is automatically controlled by ABAQUS based on the element size and material properties. The imaging area is a 0.16 m × 0.16 m square as shown in Figure 3.4. The plate thickness reduction damage is considered in this study, which is used to represent the common corrosion damage in metallic structure. The damage geometry is inscribed onto the surface of the model prior to its meshing. This ensures a uniform and structured meshing for the damage shape and helps to maintain a compatible mesh when the top layer of elements within the damage geometry are removed to create the thickness reduction damage. Inscribing the model with the damage shape prior to its meshing ensures that tetrahedral elements are used near the edges of the damage and the circular shape is maintained even after the top layer is removed.

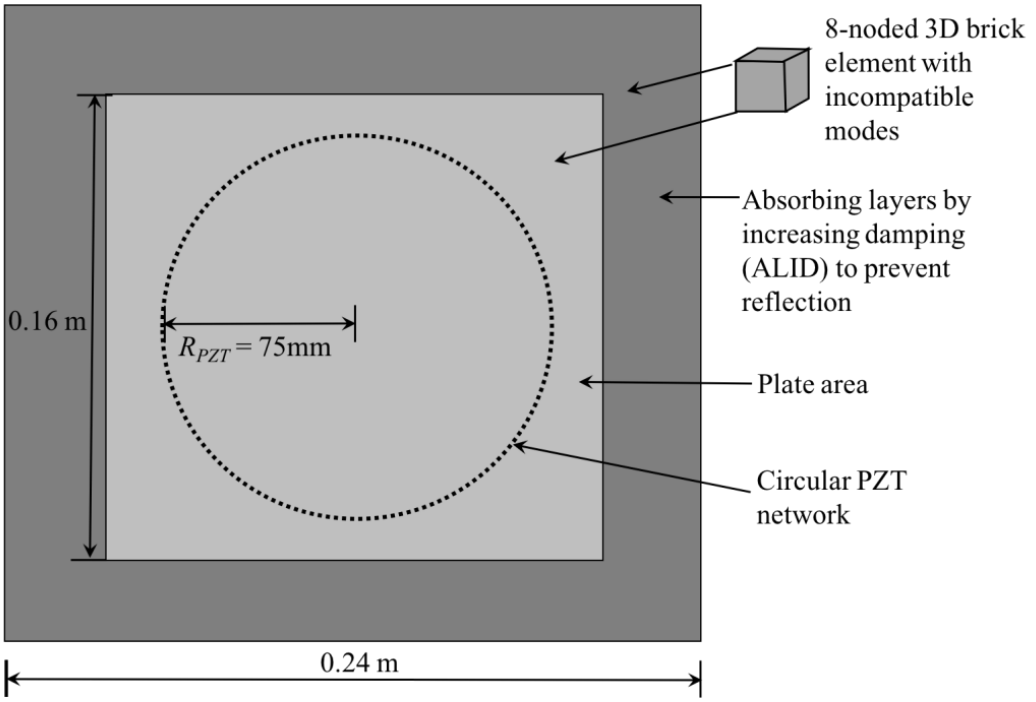

Figure 3.4: Schematic of the finite element model and the PZT configuration

In the numerical simulation, the absorbing layer is used to minimise the computational cost of the FE simulation, and hence, the simulated model can represent a larger aluminium plate. In the FE model, absorbing layers by increasing damping (ALID) [45] is applied to four edges of the aluminium plate model. A high rate of variance in the damping coefficients across the layers would give rise to stiff material layers that could themselves induce the wave reflections. A low rate of variance, on the other hand, would lead to an incomplete absorption of the incident wave, in which the boundary reflections are not fully eliminated in the simulation. It is thus imperative to vary the properties of the material gradually along these layers. The presence of an absorbing layer greatly reduces the dimension of the model to be analysed, while also eliminating any reflected waves simultaneously.

Each transducer was interrogated twice, in which one is to generate Lamb waves in an intact model and the other one is to generate Lamb waves in a model containing the damage. The scattered wave-field is then obtained by subtracting the baseline response the intact model from the total response obtained of the damaged model. The scatter field is gathered from the locations of each of the transducers and aids in constructing a single row of the multi-static data matrix K_{ij}. This process is repeated for every transducer to obtain an $N \times N$ matrix where N is the number of transducers. The diffraction tomography process requires each of the N transducers to be stimulated sequentially in order to obtain the multi-static data matrix.

The numerical studies were carried out, which considers thickness reduction damage. This paper focuses on the efficiency of various central and non-central frequencies in predicting the damage parameters for different shapes of damages. To provide a robust comparison, the damages considered in this study are located at the same location. The three cases considered in this paper are a) a circular shaped damage b) a cross shaped damage, and c) a square shaped damage. While all the cases considered are symmetric about the origin, the algorithm does not take the shape of the damage into consideration. Hence the same algorithm can be used to predict non-symmetrical damage too. Using the circular shaped damage as an example, the damage is modelled as a symmetric reduction in thickness at both surfaces of the plate as shown in Fig.3.5b. This prevents any mode-conversion [46] of waves at the damage and ensures that the scattered field consists of only the A_0 mode Lamb wave. A 10% reduction of thickness is considered in all the aforementioned cases. The image will be reconstructed at the central frequency of 200 kHz as well as at frequencies ± 20 kHz away from the central frequency.

3.4.1. Circular damage

The first case consists of a circular damage of diameter 12 mm (~ 1.5λ) located at the origin of the plate as shown in Fig. 3.5. Owing to symmetry of shape and location of the damage, the simulation of Lamb wave generation and scattering can be simplified to excitation of just one PZT. This is because the excitation of every PZT in this configuration yields the same scattered field. However, care must be taken while assembling the multi-static data matrix using Eq. 20, as the order of the elements in each row depends on order and location of the PZT excited.

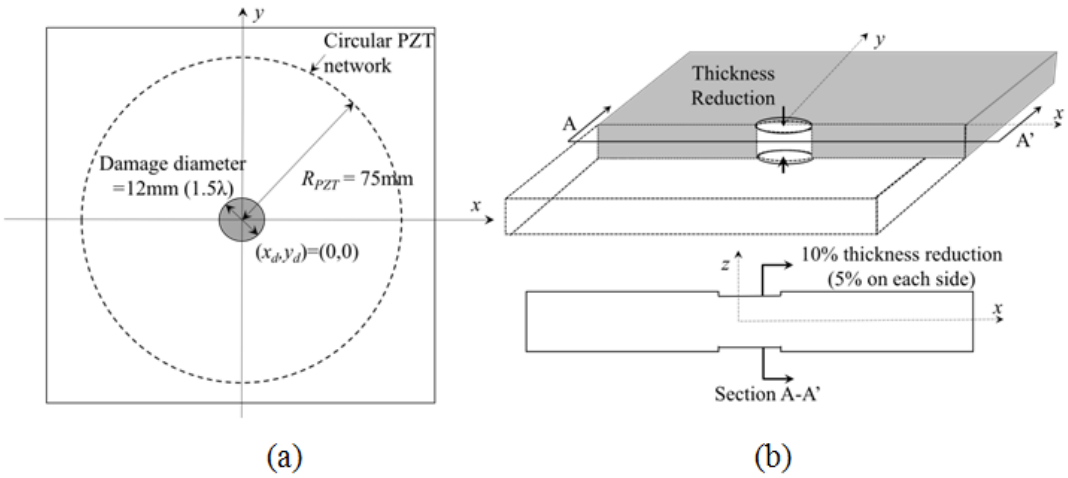

Figure 3.5: a) Schematic of the circular thickness reduction damage b) cross-section view

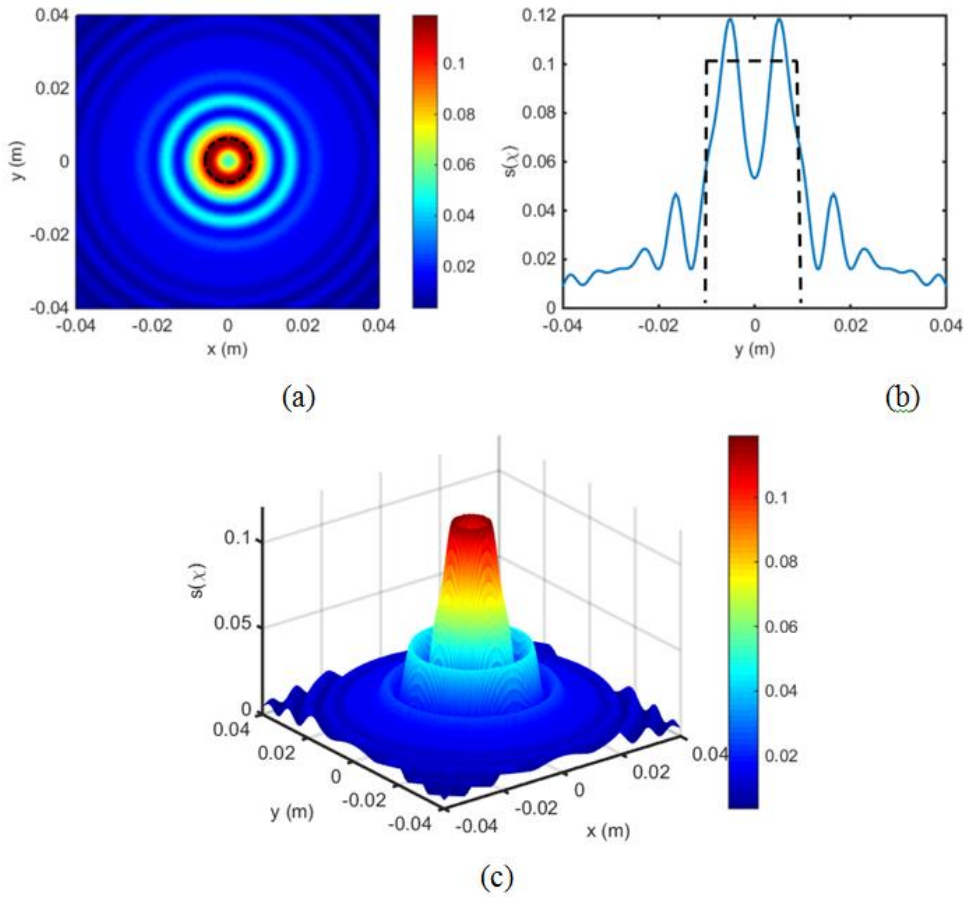

Figure 3.6: Damage reconstruction of circular damage for the central frequency of 200 kHz a) 2-D variation of damage along the surface of the plate, b) damage profile along the line x = 0, c) 3-D variation of damage (Dashed lines indicate the true geometry and thickness reduction value of the damage)

The results obtained using the algorithm, are found in Figs. 3.6, 3.7 and 3.8. The damage reconstruction was performed using the central frequency of 200 kHz, and the non-central frequencies of 180 kHz and 220 kHz. The damage reconstruction obtained using the central frequency was found to be accurate in its prediction of the thickness reduction but it was less satisfactory in its reconstruction of the damage geometry (Fig. 3.6). Figures 3.7 and 3.8 show that the use of non-central frequencies gives an excellent reconstruction of the damage

shape and size. However, they were less satisfactory in their prediction of the thickness reduction. It is worth mentioning that for non-central frequencies, while calculating the multi-static data matrix K_{ij} using the scatter data, care was taken to choose the corresponding non-central frequency in the amplitude of the actuating force as shown in Eq. 20.

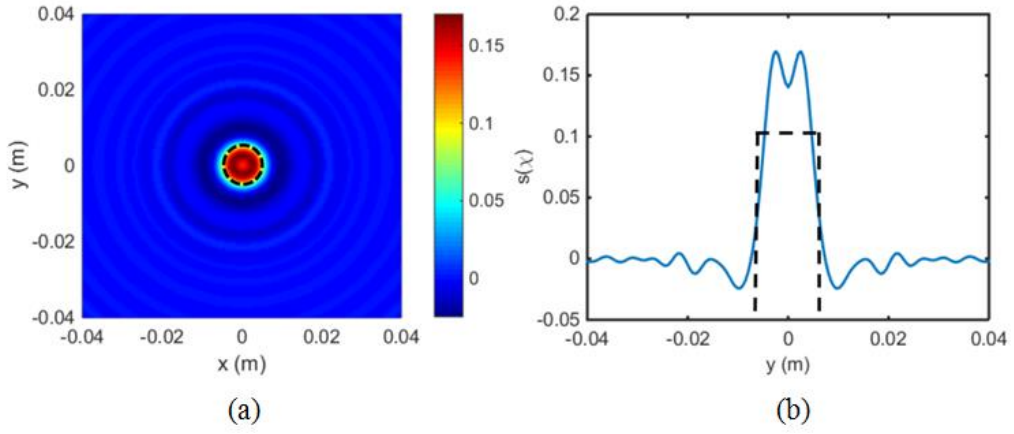

Figure 3.7: Damage reconstruction for a non-central frequency of 220 kHz a) 2-D variation, b) damage profile along the line x = 0

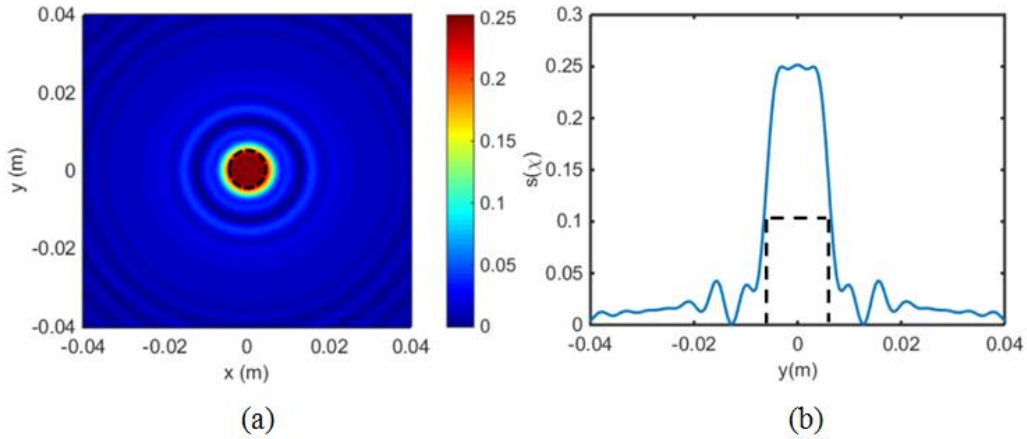

Figure 3.8: Damage reconstruction for a non-central frequency of 180 kHz a) 2-D variation b) damage profile along the line x = 0

3.4.2. Cross shaped damage

The second case consists of a cross shaped damage, located at the origin of the plate. The width of the intersecting bars is 2 mm and the total width of the cross shaped damage is 12 mm. The cross shaped damage is symmetric in each quadrant as shown in Fig. 3.9, and hence, the FE simulation can be simplified to only simulating the excitation of the 32 PZTs in the first quadrant. The results for the other 96 PZTs can be obtained by carefully rearranging the data obtained from these simulations.

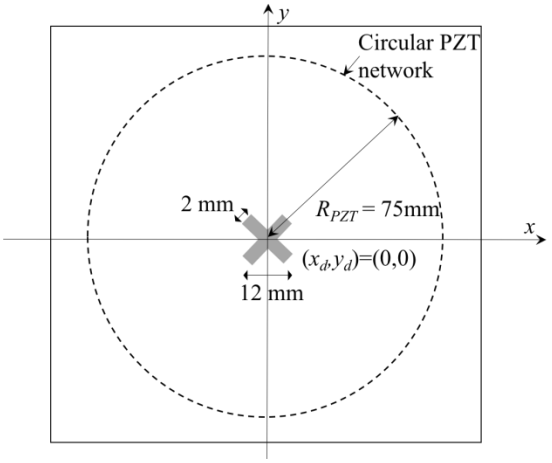

Figure 3.9: Schematic of the geometry, location and dimensions of the cross shaped thickness reduction damage

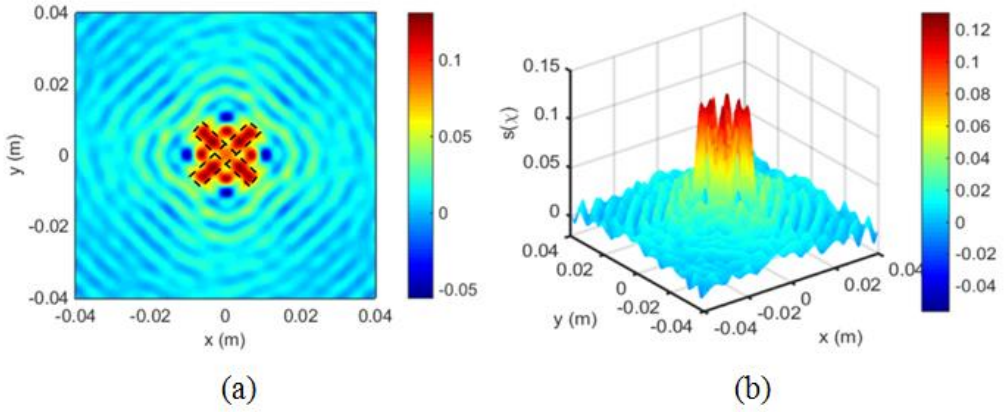

Figure 3.10: Damage reconstruction of the cross shaped damage for the central frequency of 200 kHz a) 2-D variation along the surface of the plate, b) 3-D variation along the surface of the plate (Dashed lines indicate the true geometry and thickness reduction value of the damage)

The results obtained using the imaging algorithm, are shown in Figs. 3.10 and 11. The damage reconstruction obtained using the central frequency was found to be accurate in its prediction of the thickness reduction. However, there is still some discrepancies between the reconstructed shape and the actual shape of the damage as shown in Fig. 3.10. The additional peaks between the intersecting bars can be attributed to the irregular meshing that is the result of the sharp and irregular corners in the structure. The effect of these corners can also be seen in the damage reconstruction using non-central frequencies but with lesser extent. In general, the use of non-central frequencies provides better prediction of the damage shape but the reconstructed image is less accurate in predicting the thickness reduction as well as the damage size.

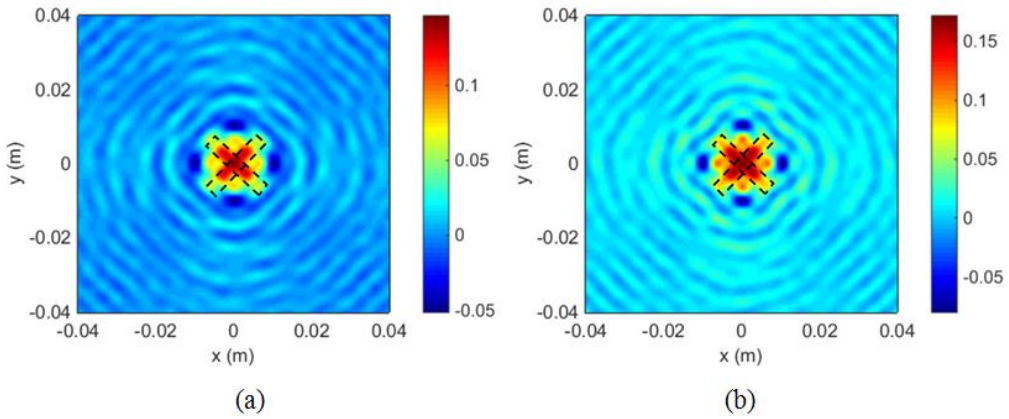

Figure 3.11: 2-D damage reconstruction of the cross shaped damage for non-central frequencies of a) 220 kHz, b) 180 kHz

3.4.3. Square shaped damage

The final case consists of square shaped damage with 12 mm wide at each side, and it is located at the origin of the plate. The same as cross shaped damage case, the square shaped damage is also symmetric in each quadrant, and hence, it be simplified to simulate only 32 PZTs. The results obtained using the imaging algorithm are shown in Figs. 3.12 and 3.13. The reconstructed images for the square shaped thickness reduction damage were found to be accurate in predicting the damage geometry and size. Although the difference in the prediction of damage geometry using both central and non-central frequencies was not as significant as in the previous cases, there was still a relatively large difference in predicting the thickness reduction. This means the performance of imaging algorithm in predicting the thickness reduction is not as good as the damage geometry and size prediction.

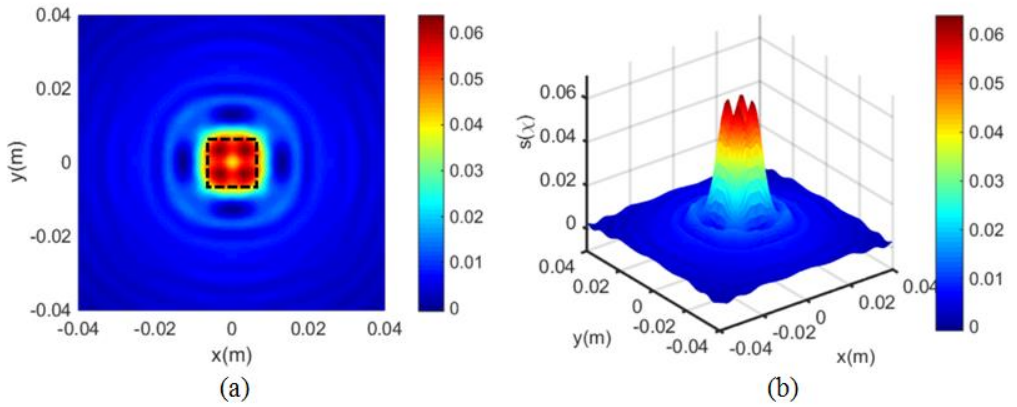

Figure 3.12: Damage reconstruction of the square shaped damage for the central frequency of 200 kHz a) 2-D variation along the surface of the plate, b) 3-D variation along the surface of the plate (Dashed lines indicate the true geometry and thickness reduction value of the damage)

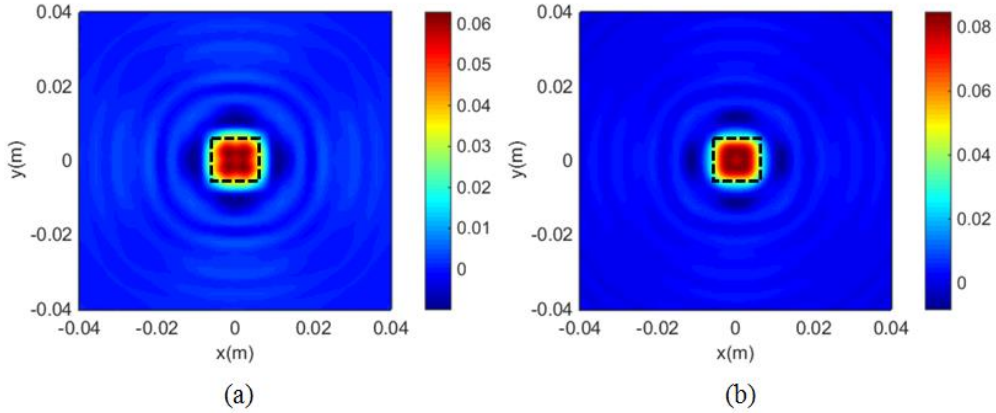

Figure 3.13: 2-D damage reconstruction of the square shaped damage for non-central frequencies of a) 220 kHz, b) 180 kHz

3.5. Conclusions

This study has investigated the performance of the LWDT in reconstructing different shapes of damage using central and non-central frequencies. A series of numerical case studies have been carried out using the 3D FE simulations. The results show that the scattering data at the non-central frequencies can also be used to reconstruct damage using LWDT. This means the non-central frequencies could provide additional information in the reconstruction of damage image. This can be attributed to the additional important information regarding the damage geometry, size or the magnitude of damage contained by each additional non-central frequency. One of the main inferences of this study is that the symmetric frequencies on either side of the central frequency provide different results in the reconstruction of the damage image. This can aid in recognising that the most efficient interval for studying multi-frequency approaches of damage reconstruction, i.e., the non-central frequency components around the centre of the frequency spectrum. The results also reconfirms that the most accurate estimations of the damage parameters are indeed obtained from the central frequencies.

In this study, it has been shown that although the central frequencies are the best sources of information in estimating the magnitude of the thickness reduction, the non-central frequencies are still helpful and can provide additional information in the image reconstruction. The quality of the damage reconstruction was found to be significantly better for regular and symmetric geometries of thickness reduction damage that do not contain sharp edges and corners. It can be observed in cross shaped damage case that while the deficiencies of the meshing and sharp corners are magnified for the central frequency, they are significantly

diminished for the non-central frequencies. Hence, one can consider an increased weighting of the contribution of non-central frequency components in the reconstruction of damage image. Efforts are currently exploiting the use of multi-frequency information in the LWDT so that the quality of the reconstructed image can be further improved.

Acknowledgement

The research described in this paper was financially supported by the Australian Research Council under grant number DE130100261. The support is greatly appreciated.

References

1. Forsyth DS, Komorowski JP, Gould RW, Marincak A (1998) Automation of enhanced visual NDE techniques. *Proc. 1st Pan-American Conf. for NDT*, Toronto, Canada 107–117.
2. Komorowski JP, Forsyth DS (2000) The Role of enhanced visual inspections in the new strategy for corrosion management. *Aircraft Eng. Aerospace Tech.*, 71(1):5-13.
3. Blitz J and Simpson G (1995) Ultrasonic methods of non-destructive testing, Springer Netherlands.
4. Schmerr LW, Song JS (2007) Ultrasonic nondestructive evaluation systems. Springer US.
5. Lepine BA, Giguere JSR ,.Forsyth DS, Chahbaz A, Dubois JMS (2002) Interpretation of pulsed eddy current signals for locating and quantifying metal loss in thin skin lap splices. *AIP Conf. Proc.* 615(1):415-422.
6. Lepine, B. A., & Holt, R. T. (1997). An eddy current scanning method for the detection of corrosion under fasteners in thick skin aircraft structures. *Canadian Aeronautics and Space Journal*, 43(1):28-33.
7. Ng, C.T. (2014). On the selection of advanced signal processing techniques for guided wave damage identification using a statistical approach. *Engineering Structures*, 67: 50-60.
8. Kurt, I., Akbarov, S.D., Sezer, S. (2016). The influence of the initial stresses on Lamb wave dispersion in pre-stressed PZT/Metal/PZT sandwich plates. *Structural Engineering & Mechanics*, 58: 347-378.

9. He, S., & Ng, C. T. (2015). Analysis of mode conversion and scattering of guided waves at cracks in isotropic beams using a time-domain spectral finite element method. *Electronic Journal of Structural Engineering*, 14: 20-32.
10. Giurgiutiu, V., & Bao, J. (2004). Embedded-ultrasonics structural radar for in situ structural health monitoring of thin-wall structures. *Structural Health Monitoring*, 3(2): 121-140.
11. Aryan, P., Kotousov, A., Ng, C. T., & Cazzolato, B. (2016). A model-based method for damage detection with guided waves. *Structural Control and Health Monitoring*, 24(3):e1884.
12. Quek, S. T., Tua, P. S., & Wang, Q. (2003). Detecting anomalies in beams and plate based on the Hilbert–Huang transform of real signals. *Smart materials and structures*, 12(3): 447-460.
13. Flynn, E. B., Todd, M. D., Wilcox, P. D., Drinkwater, B. W., & Croxford, A. J. (2011). Maximum-likelihood estimation of damage location in guided-wave structural health monitoring. *Proceedings of the Royal Society of London A: Mathematical, Physical and Engineering Sciences*, rspa2011.0095.
14. Aryan, P., Kotousov, A., Ng, C. T., & Cazzolato, B. S. (2016). A baseline-free and non-contact method for detection and imaging of structural damage using 3D laser vibrometry. *Structural Control and Health Monitoring*, 24(4):e1894.
15. Tian, Z., Yu, L., Leckey, C., & Seebo, J. (2015). Guided wave imaging for detection and evaluation of impact-induced delamination in composites. *Smart Materials and Structures*, 24(10):105019.

16. Zhao, X., Gao, H., Zhang, G., Ayhan, B., Yan, F., Kwan, C., & Rose, J. L. (2007). Active health monitoring of an aircraft wing with embedded piezoelectric sensor/actuator network: I. Defect detection, localization and growth monitoring. *Smart materials and structures*, 16(4), 1208-1217.
17. Purekar, A. S., Pines, D. J., Sundararaman, S., & Adams, D. E. (2004). Directional piezoelectric phased array filters for detecting damage in isotropic plates. *Smart Materials and Structures*, 13(4): 838-850.
18. He, S., & Ng, C. T. (2016). A probabilistic approach for quantitative identification of multiple delaminations in laminated composite beams using guided waves. *Engineering Structures*, 127:602-614.
19. He S, Ng CT (2017) Guided wave-based identification of multiple cracks in beams using a Bayesian approach. *Mechanical Systems and Signal Processing*, 84(1):324-345.
20. Sohn, H., Park, H. W., Law, K. H., & Farrar, C. R. (2007). Damage detection in composite plates by using an enhanced time reversal method. *Journal of Aerospace Engineering*, 20(3):141-151.
21. Malyarenko, E. V., & Hinders, M. K. (2001). Ultrasonic Lamb wave diffraction tomography. *Ultrasonics, 39*(4):269-281.
22. Wang, C. H., & Rose, L. R. F. (2003, March). Plate-Wave Diffraction Tomography for Structural Health Monitoring. *AIP Conference Proceedings, 657*(1):1615-1622.
23. Ng, C. T. (2015). A two-stage approach for quantitative damage imaging in metallic plates using Lamb waves, 8(4):821-841.
24. Pruell C, Kim JY, Qu J, Jacobs LJ (2009) Evaluation of fatigue damage using nonlinear guided waves. *Smart Materials and Structures*, 18(3):035003.

25. Dutta D, Sohn H, Harries KA, Rizzo P (2009) A nonlinear acoustic technique for crack detection in metallic structures. *Structural Health Monitoring*, 8(3):251-0262.
26. Soleimanpour, R., Ng, C.T. and Wang, C.H., 2017. Higher harmonic generation of guided waves at delaminations in laminated composite beams. *Structural Health Monitoring*, *16*(4), pp.400-417.
27. Shen Y, Cesnik CES (2017) Modeling of nonlinear interactions between guided waves and fatigue cracks using local interaction simulation approach. *Ultrasonics* 74:106-123.
28. Soleimanpour R, Ng CT (2017) Locating delaminations in laminated composite beams using nonlinear guided waves. *Engingeering Structures*, 131:207-219.
29. Konstantinidis G, Drinkwater BW, Wilcox PD (2006) The temperature stability of guided wave structural health monitoring systems. *Smart Materials and Structures*, 15(4):967-976.
30. Aryan P, Kotousov A, Ng CT, Wildy S (2016). Reconstruction of baseline time-trace under changing environmental and operational condition. *Smart Materials and Structures*, 25(3):035018.
31. Mohabuth M, Kotousov A, Ng CT (2016) Effect of uniaxial stress on the propagation of higher-order Lamb wave modes. *International Journal of Nonlinear Mechanics.* 86:104-111.
32. Jansen, D.P. and Hutchins, D.A. (1990). Lamb wave tomography, IEEE 1990 *Ultrasonics Symposium*, 2:871-874.

33. Malyarenko, E. V., & Hinders, M. K. (2000). Fan beam and double crosshole Lamb wave tomography for mapping flaws in aging aircraft structures. *The Journal of the Acoustical Society of America*, 108(4):1631-1639.
34. Leonard, K. R., Malyarenko, E. V., & Hinders, M. K. (2002). Ultrasonic Lamb wave tomography. *Inverse problems*, 18(6):1795-1808.
35. Rose, L. R. F., & Wang, C. H. (2004). Mindlin plate theory for damage detection: Source solutions. *The Journal of the Acoustical Society of America*, 116(1):154-171.
36. Belanger, P., Cawley, P., & Simonetti, F. (2010). Guided wave diffraction tomography within the born approximation. *IEEE transactions on ultrasonics, ferroelectrics, and frequency control*, 57(6):1405-1418.
37. Rose, L. F., & Wang, C. H. (2010). Mindlin plate theory for damage detection: imaging of flexural inhomogeneities. *The Journal of the Acoustical Society of America*, 127(2):754-763.
38. Huthwaite, P., & Simonetti, F. (2013). High-resolution guided wave tomography. *Wave Motion*, 50(5):979-993.
39. Huthwaite, P. (2014, June). Evaluation of inversion approaches for guided wave thickness mapping. Proceedings of the Royal Society of London *A: Mathematical, Physical and Engineering Sciences*, 470(2166):20140063.
40. Devaney, A. J., & Dennison, M. (2003). Inverse scattering in inhomogeneous background media. *Inverse Problems*, 19(4):855-870.
41. Rohde, A. H., Rose, L. R. F., Veidt, M., & Wang, C. H. (2009). Two inversion strategies for plate wave diffraction tomography. *Materials Forum*, 33:489-495.

42. Ng, C.T. (2015). On accuracy of analytical modelling of Lamb wave scattering at delaminations in multilayered isotropic plates. *International Journal of Structural Stability and Dynamics*, 15(8): 1540010.
43. Soleimanpour, R. & Ng, C.T. (2016). Scattering of the fundamental anti-symmetric Lamb wave at through-thickness notches in isotropic plate. *Journal of Civil Structural Health Monitoring*, 6:447-459.
44. Chan, E., Rose, L. F., & Wang, C. H. (2015). An extended diffraction tomography method for quantifying structural damage using numerical Green's functions. *Ultrasonics*, 59:1-13.
45. Rajagopal, P.,Drozdz, M., Skelton, E.A., Lowe, M.J.S., Craster, R.V. (2012) On the use of absorbing layers to simulate the propagation of elastic waves in unbounded isotropic media using commercially available Finite Element packages. *NDT & E International*, 51**,** 30–40.
46. Ng, C.T. (2014). Bayesian model updating approach for experimental identification of damage in beams using guided waves. *Structural Health Monitoring*, 13(4): 359-373.

Chapter 4

4. Multi-frequency methods for the reconstruction of damages in plate like structures

(Paper 3, Under preparation)

Gnana Teja Pudipeddi

Graduate Student, School of Civil, Environmental and Mining Engineering, The University of Adelaide, Adelaide, South Australia, 5005, Australia.

Email: gnanateja.pudipeddi@adelaide.edu.au

Ching-Tai Ng

Associate Professor, School of Civil, Environmental and Mining Engineering, The University of Adelaide, Adelaide, South Australia, 5005, Australia (Corresponding author).

Email: alex.ng@adelaide.edu.au

Andrei Kotousov

Professor, School of Mechanical Engineering, The University of Adelaide, Adelaide, South Australia, 5005, Australia.

Email: andrei.kotousov@adelaide.edu.au

Publication:

Pudipeddi, G. T., Ng, C. T., & Kotousov, A. Multi-frequency methods for the reconstruction of damages in plate like structures. **(Under preparation)**

Statement of Authorship

Title of Paper	Multi-frequency methods for the reconstruction of damages in plate like structures.
Publication Status	☐ Published ☐ Accepted for Publication ☐ Submitted for Publication ☑ Unpublished and Unsubmitted work written in manuscript style
Publication Details	Pudipeddi, G. T., Ng, C. T., & Kotousov, A. Multi-frequency methods for the reconstruction of damages in plate like structures.

Principal Author

Name of Principal Author (Candidate)	Gnana Teja Pudipeddi
Contribution to the Paper	Performed literature review and researched the topic, developed numerical models and studied various shapes and cases of damage, studied different imaging methods and developed models using the said methods, analysed and drew conclusions from the results, prepared the manuscript
Overall percentage (%)	80%
Certification:	This paper reports on original research I conducted during the period of my Higher Degree by Research candidature and is not subject to any obligations or contractual agreements with a third party that would constrain its inclusion in this thesis. I am the primary author of this paper.
Signature	Date 03/07/2019

Co-Author Contributions

By signing the Statement of Authorship, each author certifies that:

i. the candidate's stated contribution to the publication is accurate (as detailed above);

ii. permission is granted for the candidate in include the publication in the thesis; and

iii. the sum of all co-author contributions is equal to 100% less the candidate's stated contribution.

Name of Co-Author	Ching Tai-Ng
Contribution to the Paper	Supervised development of work and reviewed and corrected draft of manuscript
Signature	Date 11/7/2019

Name of Co-Author	Andrei Kotousov
Contribution to the Paper	Supervised development of work and reviewed and corrected draft of manuscript
Signature	Date 11/7/2019

Please cut and paste additional co-author panels here ~~as required~~.

Abstract

This paper proposes a multi-frequency framework for improving the cost-efficiency and viability of Lamb Wave Diffraction Tomography (LWDT) in damage image reconstruction. The proposed imaging algorithm incorporates the non-central frequency data of the measured scattered wave field to provide additional information in the damage image reconstruction. The advantage of using non-central frequency data for damage image reconstruction is that it not only reduces the number of transducers used for capturing the scattered wave fields, but also avoid compromising the image quality. Therefore, the proposed method can significantly increase the viability of LWDT in the damage image reconstruction.

A series of case studies considering different levels and shapes of thickness reductions in aluminium plates are used to demonstrate the capability and performance of the proposed multi-frequency framework for LWDT. In this study, two different numerical schemes are considered in the damage image reconstruction. The results show that the multi-frequency approach has a significant improvement in the quality of image over the traditional single frequency approach. In addition, the number of transducers required for the damage image reconstruction can be significantly decreased without reducing the quality of the reconstructed damage images.

Keywords:

Lamb wave, diffraction tomography, imaging, multi-frequency, damage identification, structural health monitoring, scattering

4.1. Introduction

Structural health monitoring (SHM) of plate-like structures is of special interest to researchers due to the ubiquity of curved and thin-walled structures in everyday life. These structures have been frequently used in different industries, such as defence, aerospace, oil and gas, shipping and automotive industry etc. Structural safety and integrity of structures are of utmost importance owing to the significant physical, economic and environmental consequences can occur if structural failure happens caused by the damage. Different non-destructive evaluation (NDE) techniques, such as visual inspection, radiography, eddy-current and conventional ultrasonic [1, 2], were developed and used to ensure the structural safety and integrity of structures.

In the literature, ultrasonic guided waves have been widely recognized as one of the promising approaches for damage detection owing to its high sensitivity for detecting damage in structures. Ultrasonic Lamb wave is a particular type of guided waves that propagates in thin plate. Lamb wave is stress wave propagating along the structure and its propagation characteristics are governed by the boundaries of the structure [3]. The advantages of Lamb wave are its ability to travel large distances with minimal dissipation and high sensitivity to small and different types of damage.

4.2. Inverse problems

Various algorithms were developed to translate Lamb wave signals into accurate quantification of damage. These algorithms can be broadly classified into two categories, forward algorithms and inverse algorithms [9]. The forward algorithm

involves the calculation of a response or behaviour of a system from the characteristics of the input data. Obtaining the behaviour of a structural system from its physical properties and the applied force is an example of the forward problem. In the forward problem, the physical properties are modelled, and the results of a simulation are compared to the data that obtained in experiment. In SHM, the time-of-flight (ToF) approach is one of the simple examples of the forward algorithm. In this approach, the location of the damage is estimated based on the difference between the travelling times of the incident signal and the signal reflected by the damage. The ToF information can be used to identify the location of the damage.

The inverse algorithm, on the other hand, use the observed data to estimate the unknown physical properties that give rise to the data. Inverse problems are widely studied in the field of engineering, where the data can be accurately measured but the system properties that lead to this data are hard to be estimated. Inferring the seismic behaviour of earth's subsurface based on the recordings measured on its surface is an example. In some of the fields, the inverse problems are a constant topic of research areas, such as oceanography, remote sensing, optics, signal processing and machine learning. Medical imaging and computer vision are some of the most active fields of research for these problems because of the nature of the problem in these fields. Computed tomography, for example, requires generating an image of the visceral organs within a human body, based on the property of the body to absorb X-rays that passed through it. Diffraction tomography is another process that makes use of a similar principle to reconstruct the geometry of damage within a structure.

4.2.1. Lamb wave diffraction tomography

Different Lamb wave based damage detection techniques were developed in the literature. In particular, Lamb wave diffraction tomography (LWDT) has attracted significant research interests in last few years. One of the advantages of the LWDT in damage detection is that it can provide quantitative information of the damage by reconstructing an image to indicate the shape and size of the damage, which provide essential information to support engineers in assessing the risk of the damage to the structural safety, making decision on the remedial work, and predicting remaining life of the structure.

For isotropic materials, Wang and Rose [4] proposed a LWDT framework based on the Mindlin plate theory and Born approximation, which relates the scattered plate waves to the damage geometry [5]. The damage parameters are mathematically represented as local perturbations of the global material parameters. The scattered field amplitudes were then found to have a linear relationship with the Fourier transform of these perturbation functions. Hence, once the Fourier transform values of the perturbations are obtained from the scattered field amplitudes, an inverse transformation can be applied to obtain the damage parameters [5]. The framework was implemented and extended by Vedit et al. [6] and Ng et al. [7] on a flat isotropic plate. Another non-iterative guided wave imaging method, based on an acoustic model for wave propagation, was developed by Huthwaite and Simonetti in the context of breast imaging [19, 20, 21]. They developed a hybrid algorithm based on the time-of-flight method with diffraction tomography. Huthwaite [22] also studied the performance of this approach using scattered data that was obtained computationally from (i) an acoustic model, and (ii) a finite element (FE) model. The scatter data obtained

from the FE model was found to give rise to images of a higher resolution when compared to the data obtained from the acoustic model. This was largely due to the inability of acoustic models to accurately simulate guided wave scattering in elastic plates.

Development of accurate and simple inverse transformation techniques that do not require a large number of transducers is a very important topic in this research area. In addition to the inverse Fourier transformation, Devaney and Dennison [8, 9] proposed a least-squares estimation method for inverse transformation. The least-squares estimation method was studied by Rohde et al. [5] using a constrained linear inversion technique and the results were found to be more accurate and show better performance than the direct Fourier inversions [5].

One of the major requirements for the technique suggested by Wang and Rose is the assumption that the scattered field data collected is under far-field conditions. That is, the distance between the transducers and the damage is greater than $2d^2/\lambda$ [10, 11] where 'd' is the diameter of the damage and 'λ' is the wavelength of the incident wave. However, a near-field imaging method is more practical as the damage may be located close to the transducers in real life applications. This limitation was addressed by Chan et al. [11] where they employed numerical solutions to the Green's functions and a near field multi-static data matrix to overcome this constraint. Green's function is an undamaged structural response due to a unit input [11] and its solution is usually difficult to obtain analytically. However, the Green's function can be computed using numerical simulation techniques, e.g. finite element simulation. In this paper, we utilize the numerical calculated Green's functions in the proposed multi-frequency LWDT framework.

The LWDT algorithm presented in the study of Pudipeddi et al. [12] only used the central frequency components of the incident wave in the damage image reconstruction. Although the central frequency data of the signal is predominant and has maximum amplitude in the frequency-domain, it can be observed that the signal also contains multiple frequency data adjacent to the central frequency. These multiple frequency data can be utilized to provide extra information in the damage image reconstruction. A multi-frequency approach that incorporates multiple frequencies in the damage image reconstruction was proposed by Devaney and Dennison [9]. But their study was limited to acoustic wave. Belanger et al. [13] also studied this phenomenon at a later stage. However, the potency of this algorithm in reducing the number of transducers used, without compromising on the image quality was not studied in detail.

The aims of this paper is to study the image reconstruction algorithm using a multi-frequency framework to achieve lesser number of transducers and better image resolution. In addition, different to the approach proposed by Devaney and Dennison [9] and Belanger [13], the multi-frequency LWDT framework is developed based on the Mindlin plate theory. In this study, two different linear inversion techniques are used to obtain the solution. The non-central frequency data of the scattered wave field is utilized in the proposed multi-frequency approach for damage image reconstruction. The effect of multiple frequency data on the quality of the damage image reconstruction is studied in detail. In addition, the quality of the reconstructed damage image obtained by the multi-frequency approach is compared with that of using single frequency approach.

The rest of this chapter is organized as follows. Section 2 is the methodology that describes the details of the proposed multi-frequency LWDT

framework. The results of a series of numerical case studies are used to demonstrate the performance of the multi-frequency framework in Section 3. The results and inferences obtained from this study are stated in Section 4.

4.3. Methodology

Mathematically, an inverse problem can be represented in the following form:

$$d = g(m) \tag{1}$$

where d is a parameter based on the observed data and g is the forward mapping from the physical parameter m to the observed data. In a special case where mapping g is linear in nature and d consists of a discrete set of parameters. Eq. 1 takes the form of a linear system of equations

$$\boldsymbol{d} = \boldsymbol{Gm} \tag{2}$$

where $\boldsymbol{d}$ now takes the form of a vector of size N_1 obtained from the observed data, $\boldsymbol{m}$ is a vector of unknown quantities with size N_2, and $\boldsymbol{G}$ is a matrix of size N_2 x N_1. Owing to the difference in sizes of vectors $\boldsymbol{d}$ and $\boldsymbol{m}$, these system of equations seldom have a unique solution and require iterative methods to obtain a solution.

Imaging techniques, especially tomographic methods, have been found to be one of the most commonly used techniques in solving the linear inversion problems. It is an area of study for mathematicians and engineers. Research in this topic has led to algorithms for various processes, such as X-ray computed tomography, diffraction tomography and Doppler tomography. An in depth

discussion of the mathematical background and formulation for the process of diffraction tomography has been addressed in multiple publications [4, 5, 8, 9, 14-16]. The process and equations are summarised in the following sections.

At any given frequency ω, the imaging algorithm takes the form of the inverse problem discussed above, by mapping the scatter data obtained to a discrete complex valued scattering potential $O(r, \omega)$. The damage is interrogated by N piezoelectric transducers that serve as both activating and receiving sensors, and lead to an N x N multistatic data matrix. This multistatic data matrix is obtained from the measured scattered field by taking the Fourier transformation of the scattered wave field, normalized relative to the amplitude of the actuating force at the central frequency of the input tone-burst [9, 11, 12].

$$K_{r,s}(\omega) = \frac{\hat{w}^S(N_r,\omega;N_s)}{\hat{F}(\omega_c)} \tag{3}$$

where $\hat{w}^S$ is the scatter wave field obtained by interrogating the damage with an incident wave from source N_s, as measured by a receiver N_r. ω_c is the central frequency of the input tone-burst. Rearranging the terms of the multistatic data matrix to form a vector, we get

$$d_i(\omega) = K_{r,s}(\omega) \tag{4}$$

where $i = r + (s-1)N$ and $r, s = 1,2,3, \ldots . N$. The size b of vector $\boldsymbol{d}$ is thus N x $N = N^2$. For any given frequency, the scattered data matrix $\boldsymbol{d}$ is related to the discrete scatter potential matrix $\boldsymbol{O(\omega)}$, by a linear mapping $\boldsymbol{G}$

$$G = \int_v d^3r\, \pi_i^*(r,\omega) \tag{5a}$$

with

$$\pi_i(r,\omega) = \begin{cases} G_0^*(N_r, r, \omega) G_0^*(N_s, r, \omega) & \text{if r } \in \nu \\ 0 & \text{otherwise} \end{cases} \quad (5b)$$

where v is the volume enclosing the scattering object and G_0 is the Green's function of the background medium. Thus the problem, when expressed in the form of Eq. 2, becomes

$$GO(\omega) = d_i(\omega) \quad (6)$$

Substituting Eq. 5a into Eq. 6, it gives

$$d_i(\omega) = \int_v d^3r\, \pi_i^*(r,\omega) O(r,\omega) \quad (7a)$$

But

$$\int_v d^3r\, \pi_i^*(r,\omega) O(r,\omega) = \langle \pi_i, O(r,\omega) \rangle_{H_v} \quad (7b)$$

where $\langle \pi_i, O(r,\omega) \rangle_{H_v}$ is the standard inner product in the Hilbert space $\boldsymbol{H_v}$**.** The pseudo-inverse solution to the scattering problem is then given by [8, 17]

$$\hat{O}(r,\omega) = \sum_{i=1}^{N^2} C_i\, \pi_i(r) \quad (8a)$$

where coefficients C_i are solutions to the equation

$$d_i(\omega) = \sum_{i'=1}^{N^2} C_{i'} \langle \pi_i, \pi_{i'} \rangle_{H_v} \quad (8b)$$

Eq. 8b can be written matrix form, as: [8, 9]

$$\boldsymbol{\Pi C} = \boldsymbol{d} \quad (9)$$

where $\prod$ is an M x M inner product matrix, and $\boldsymbol{C}$ and $\boldsymbol{d}$ are vectors of size M.

4.3.1. Multi-frequency framework

Devaney and Dennison [9] first showed the potency of using a multi-frequency approach in improving the quality of an image. They incorporated multiple central frequency data into their inversion algorithm and studied the resolution of the reconstructed image. It was found that an increasing in the number of central frequencies largely have the same effect as an equivalent increase in the number of sensors [9]. However, their framework involved using multiple central frequency data, i.e. multiple excitation frequencies. This means the corresponding increase in the logistics of implementing the damage detection as the excitation would need to be repeated as many times as the number of excitation frequencies considered. This study examines the use of non-central frequency data in damage image reconstruction, and hence, it avoids the need of multiple excitations. It also studies the variation in the quality of the image with reduction in the number of transducers and increase in the number of frequency components. This demonstrates the feasibility of reducing the number of transducers without significantly altering the quality of image.

Use of numerical Green's functions [11] plays an important role in this framework as this not only extends the algorithm to include near field imaging, but also gives a computationally efficient way to obtain the Green's functions for multiple frequencies. The use of scattered field to develop the multistatic data matrix in Eq. 3 ensures the matrix for the multi-frequency framework can be implemented with ease and efficiency. The multi-frequency framework is similar to the single frequency framework in its structure [8, 9]. The mathematical effect of incorporating multiple frequencies is the same as that of incorporating multiple

transducers. Thus, with the inclusion of N_ω multiple frequencies, Eq. 4 has the form

$$d_i(\omega) = K_{r,s}(\omega) \tag{10a}$$

where

$$i = r + (s-1)N + (f-1)N_\omega \; ; \qquad r, s = 1, 2, 3, \ldots . N;$$

$$f = 1, 2, 3 \ldots N_\omega$$

(10b)

The size M of vector $\boldsymbol{d}$ is thus

$$M = N \times N \times N_\omega \tag{11}$$

Correspondingly, the value of i in equations 5, 6, 7 and 8 would also vary from 1 to M.

It can be observed from Eqs. 9 and 10 that the system of linear equations may either not have a solution, or not possess a unique solution [8, 9]. Devaney and Dennison [8,9] addressed this issue by using the least squares method to obtain a solution. Additionally, we have used the algebraic reconstruction technique (ART) to develop an iterative solution for the system of linear equations. The least squares method and ART were compared in terms of the computational efficiency and advantages. The following section gives a brief overview of the ART.

4.3.2. Algebraic reconstruction technique

ART is an iterative method that was first developed in the context of image reconstruction by Gordon, Bender and Herman [18]. The same method is called

the Kaczmarz method in the field of linear algebra. For a given system of linear equations $= \boldsymbol{d}$; where $\boldsymbol{G}$ is a matrix of size m x n, the (k+1) iteration of solution $\boldsymbol{m}$ is obtained in the following manner:

$$m_{k+1} = m_k + \lambda_k \frac{d_i - \langle g_i, m_k \rangle}{\|g_i\|^2} g_i^T \tag{12}$$

where $i = (k \; mod \; m) + 1$; g_i is the i^{th} row of matrix $\boldsymbol{G}$; $\boldsymbol{d_i}$ is the i-th component of vector $\boldsymbol{d}$ and λ_k is a relaxation parameter. The following section provides a discussion of the numerical analysis performed on three different damage cases. The inverse imaging problem was solved by both least squares method and ART for all the damage cases. The image quality obtained using 32 transducers is compared to the image quality obtained using 64 transducers. Finally, additional non-central frequencies on either side of the central frequency (Figure 4.1) are used to develop a multi-frequency approach for damage image reconstruction. The quality of this image is then studied with reference to the image obtained using single central frequency data.

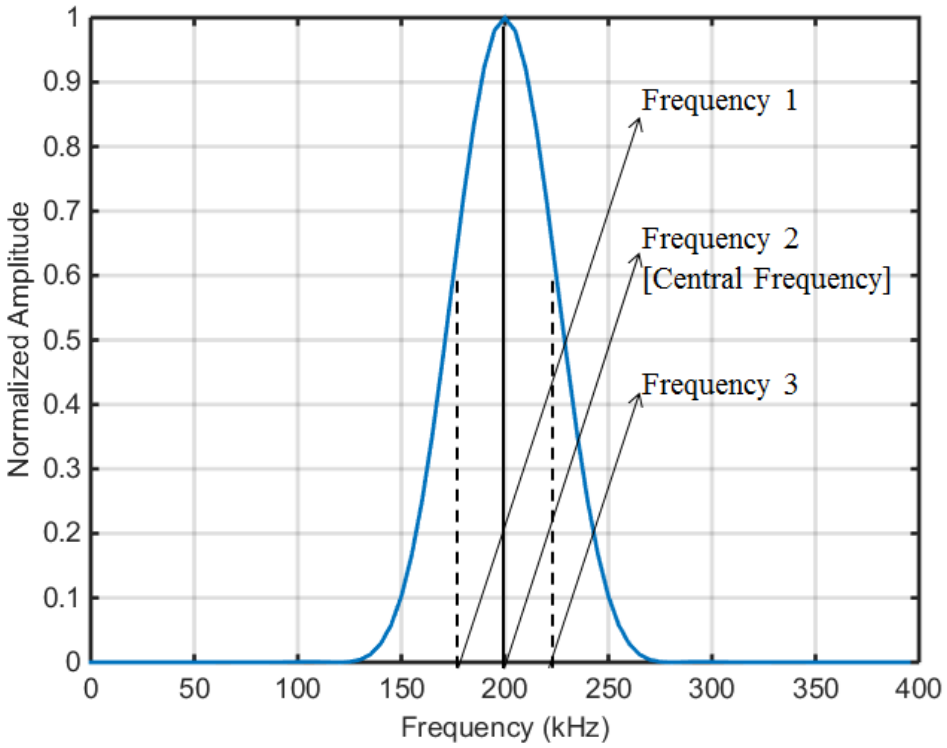

Figure 4.1: The three frequency components in the Fourier transform of a Lamb wave signal at 200 kHz, that are used to develop the multi-frequency approach

4.4. Numerical case studies

The inversion techniques and multi-frequency approach are demonstrated using an isotropic aluminium plate [12]. The details of the model are summarised in Table 4.1.

Table 4.1: Properties of the numerical simulation model

Model Parameter	Value
In-plane dimensions	240 mm × 240 mm
Thickness	1.6mm
Young's modulus	69 GPa
Density	2760 kg/m^3
Poisson's ratio	0.33
Element type	Eight-noded 3D reduced integration solid brick element (C3D8I) with incompatible modes
Excitation signal	200 kHz narrow-band five-cycle

	sinusoidal tone burst modulated by a Hanning window
Wave length of the A_0 Lamb wave	7.5 mm
Wave mode	Anti-symmetric (A_0)
In-plane element size of the FE model	0.4 × 0.4 mm^2

The radius of the circular transducer network used to interrogate the damage is 10λ = 75 mm. The 160 mm × 160 mm square imaging area is shown in figure 4.2. The plate thickness reduction damage is considered in this study and it is symmetric about the mid-plane of the plate.

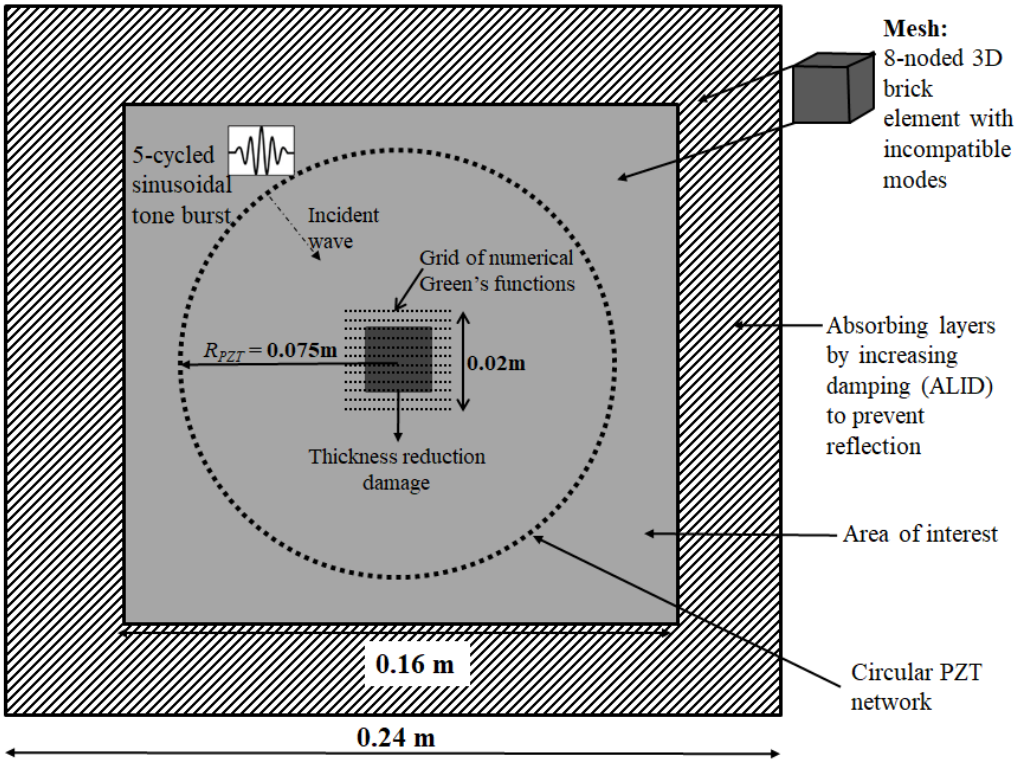

Figure 4.2: Schematic of the finite element model and the transducer configuration

A series of numerical studies were carried out and they consider three different damage cases. a) A square shaped damage b) A cross shaped damage and c) An off-centre circular damage. A 10% reduction of thickness is considered

in all the aforementioned cases. The image was reconstructed using the data at the central frequency of 200 kHz as well as at frequencies ± 20 kHz of the central frequency as shown in Fig. 4.1.

4.4.1. Numerical Green's function

Numerical Green's functions can be used in the LWDT algorithm to achieve the near-field imaging [11] and can be extended for multi-frequency approach. The Green's function for a point x from a sensor X_i is given by:

$$G(x, X_i) = \frac{\hat{w}^S(x, X_i, \omega)}{\hat{F}(\omega)}$$

(13)

where $\hat{w}^S$ and $\hat{F}$ are the Fourier transforms of the scattered field and input force at frequency ω. Since the principle of reciprocity applies to these Green's functions,

$$G(x, X_i) = G(X_i, x)$$

(14)

Thus, these functions need only to be calculated for a grid of points, from each of the sensors [11]. The spacing between each of the points needs to be less than $\lambda/2$. Since the wavelength λ of the anti-symmetric wave at frequency 200 kHz is 7.5mm, a grid with spacing of 3 mm was taken for this model. The imaging domain was taken to be a square of side 15mm or 30 mm (depending on the size and location of the damage) centred at the origin of the plate, for the sake of computational convenience.

4.4.2. Square shaped damage

The first damage case is a square shaped damage with dimensions of 12 mm x 12 mm, and located at the origin of the plate as shown in Fig. 4.3. The multi-frequency framework is used to reconstruction an image for this damage using the least squares pseudo inverse method and the ART, respectively. In each of the methods, three different combinations of transducers and frequencies were studied.

Case i: 32 transducers with single frequency data (200 kHz)

Case ii: 64 transducers with single frequency data (200 kHz)

Case iii: 32 transducers with multi-frequency (180 kHz, 200 kHz and 220 kHz)

Cases i and ii are used to study the effect of number of transducers on quality of the reconstructed damage image. Cases i and iii are used to demonstrate the advantages of a multi-frequency framework. The colour-bar in the plot represents the resolution or intensity of damage and it is the normalized value of the damage parameter obtained from the calculation.

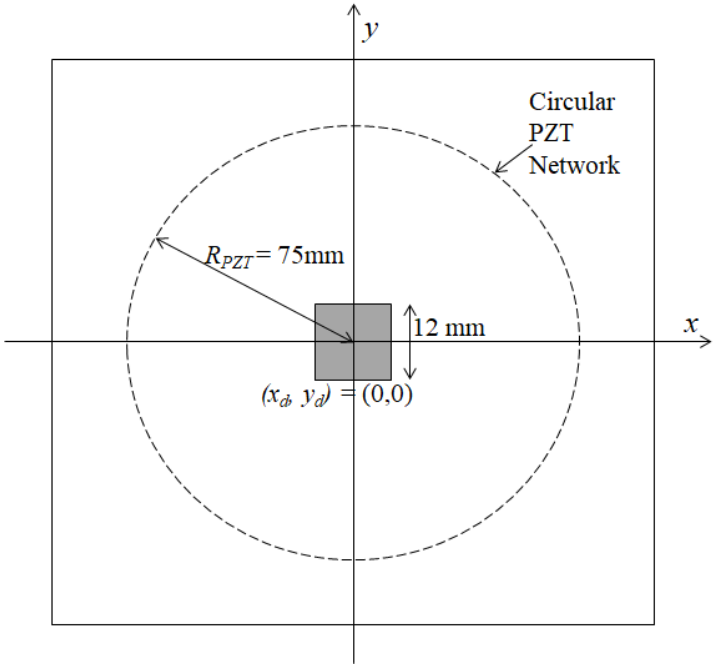

Figure 4.3: Schematic of the geometry, location and dimensions of the square shaped thickness reduction damage

Least squares method

The results obtained using the least squares pseudo inverse procedure are as follows. Figure 4.4a shows the results obtained using single frequency data measured by 32 transducers (**Case i**). The results of single frequency data measured by 64 transducers (**Case ii**) are shown in Figure 4.4b. The multi-frequency data measured by 32 transducers (**Case iii**) are shown in Figure 4.4c.

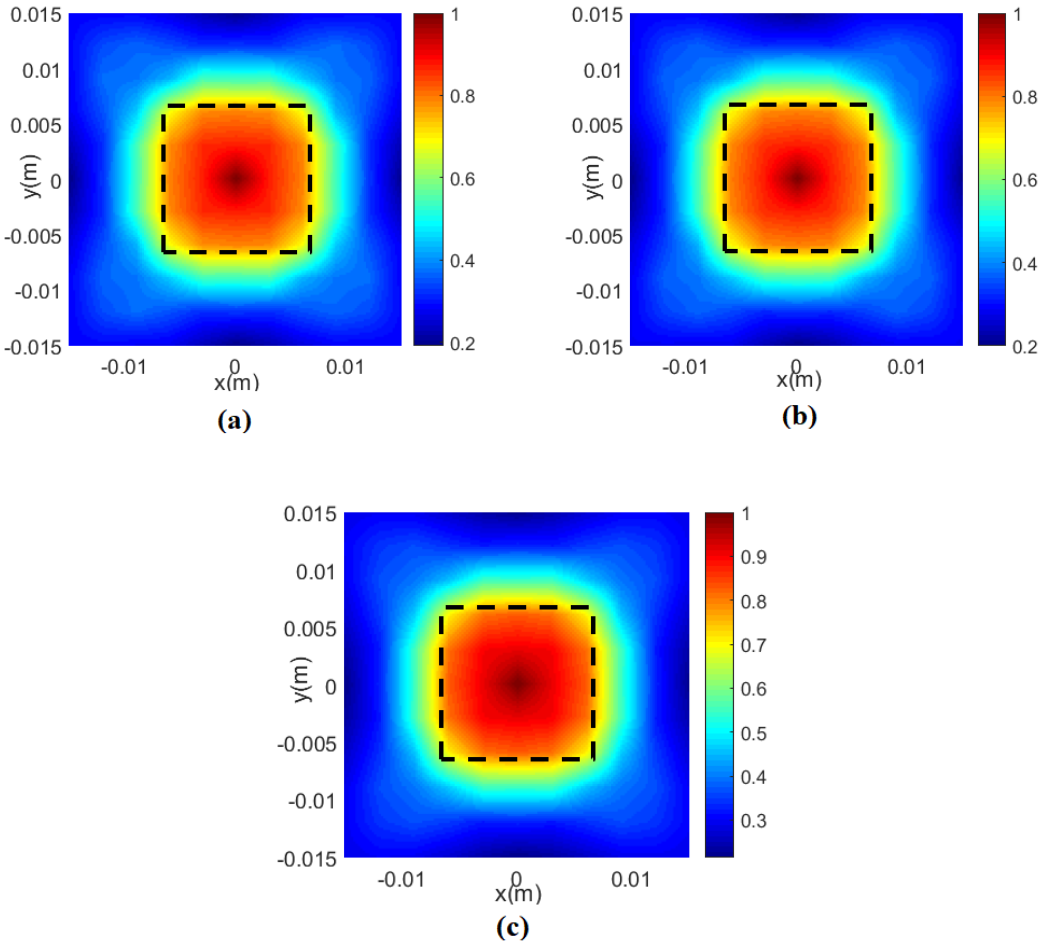

Figure 4.4: Reconstructed square shaped damage image using least squares method for a) Case i, b) Case ii and (c) Case iii. Dashed lines indicate true geometry of square shaped damage

It can be observed that the effect of increasing transducers has a very small effect on the damage quality in this case. Careful observation of the images also shows that the multi-frequency approach has a slightly higher accuracy of the shape and size of the reconstructed damage (darker shade of red in the damage area). Thus, the results using multi-frequency data measured by 32 transducers have a slightly better performance than the single frequency case.

Algebraic reconstruction technique

The results obtained using ART are found to have a much better prediction of the damage shape when compared to the results obtained using least squares method. The effect of increasing the number of transducers is marginal when compared to the effect of using multiple frequency data in the damage image reconstruction. Figures 4.5a and 4.5b show the reconstructed damage image using single frequency data (200 kHz) measured by 32 transducers and 64 transducers, respectively. Figure 4.6 shows the reconstructed damage images at different number of iterations in ATR using multi-frequency data measured by 32 transducers.

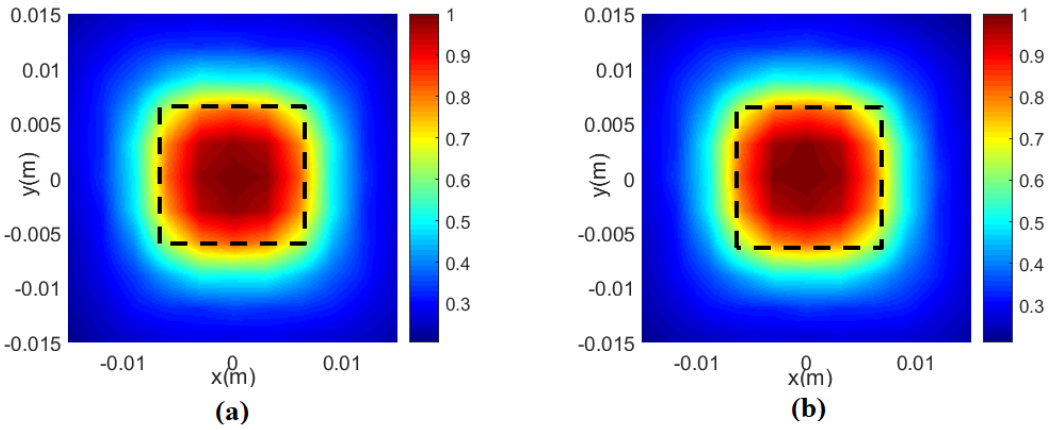

Figure 4.5: Damage image reconstruction of a square shaped damage using ART for a) Case i and b) Case ii. Dashed lines indicate the true geometry of damage

It can be shown that the reconstructed image at around 3000 iterations is converged to a constant shape and dimension. Although the ART method has better performance in predicting the damage shape in the cases using single frequency and multi-frequency, it is still computationally cumbersome compared to the least squares method.

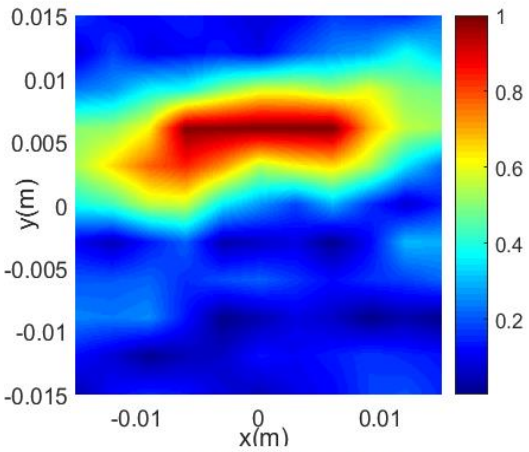

Iterations = 500

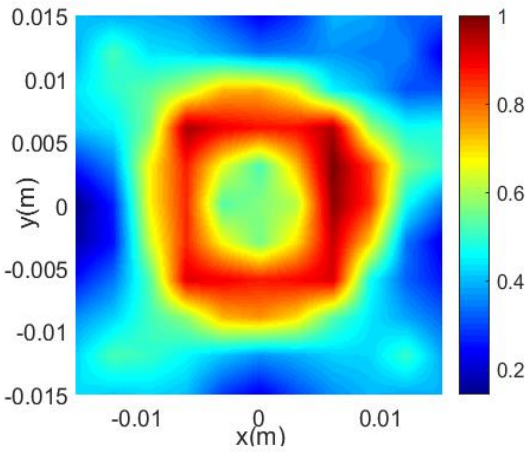

Iterations = 1000

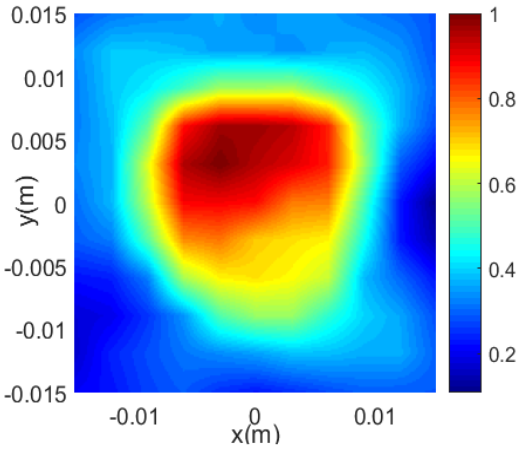

Iterations = 1500

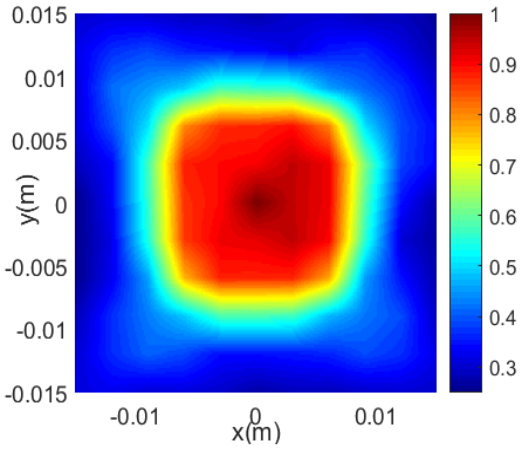

Iterations = 3000

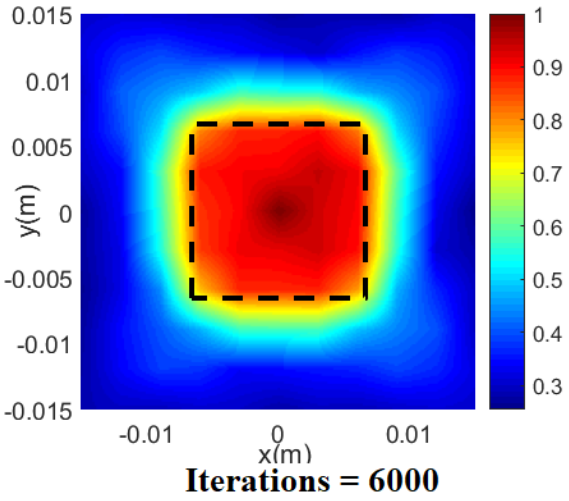

Figure 4.6: Reconstructed square shape damage image at different numbers of iterations using ART and multi-frequency data measured by 32 transducers. Dashed lines indicate true geometry of the damage

4.4.3. Cross shaped damage

The two inverse methods discussed above are implemented on a different shape of damage. It is a 2 mm thick criss-crossing strip of thickness reduction damage, as shown in Fig. 4.7. Three cases are considered, they are 32 transducers with a single frequency, 64 transducers with a single frequency, and 32 transducers with multiple frequencies.

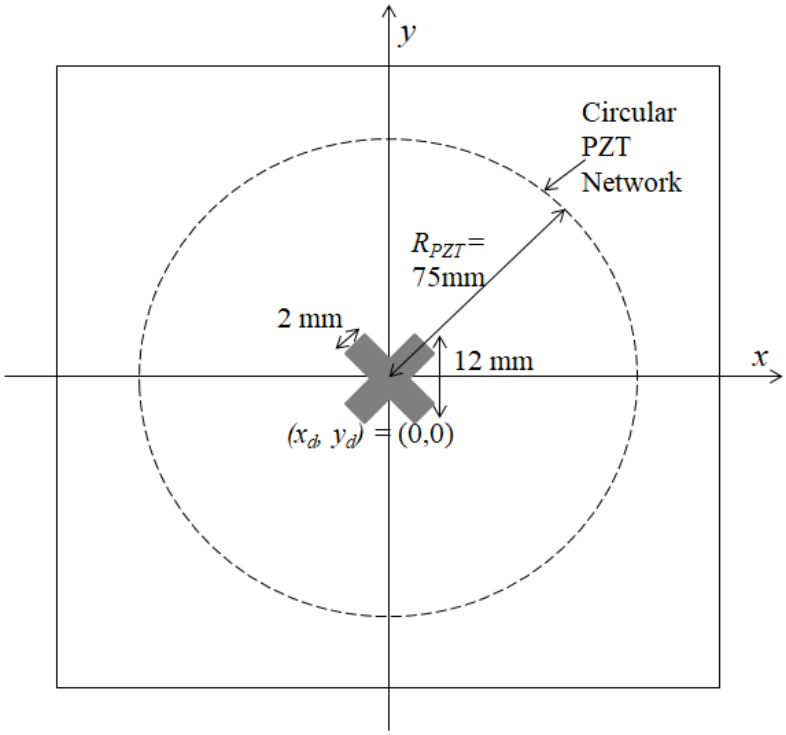

Figure 4.7: Schematic of the geometry, location and dimensions of the cross shaped thickness reduction damage

Least squares method

The results obtained using the least squares method shows a clear pattern that matches with the corresponding results obtained for the square shaped damage. However, in this case, Fig 4.8a and 4.8b also show that the 64 transducers single frequency case for this damage has a markedly better prediction than the 32 transducers single frequency case. Thus, in addition to showing that the use of multiple frequencies gives rise to a better damage image reconstruction (Fig. 4.8c), the effect of increasing number of transducers on the damage quality is investigated. A key observation in this case is the skew in the image of the damage. It can be seen that the image is slightly rotated in the anti-clockwise direction. The irregularities in the constructed image can be attributed to the complex nature of the damage shape, which has multiple sharp edges and angles.

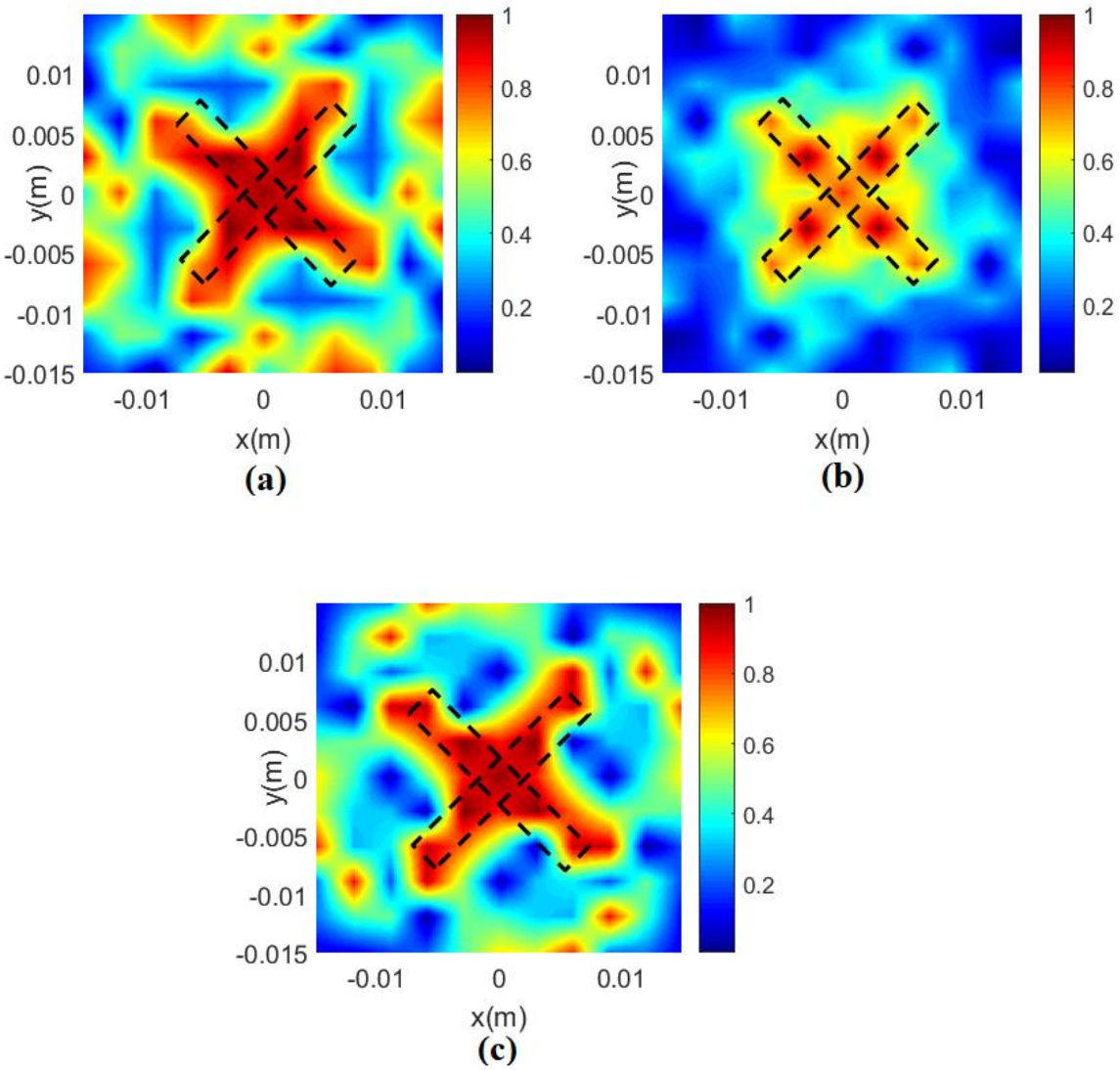

Figure 4.8: Damage reconstruction of a cross shaped damage using least squares method for a) Case i, b) Case ii and (c) Case iii. Dashed lines indicate true geometry of damage

Algebraic Reconstruction Technique (ART)

The results obtained using ART for the cross shaped damage are found to be less accurate than the results obtained using the least squares method. They, however, continue to follow the pattern of showing a better performance for the multi-frequency approach over the single frequency case (Figs. 4.9 and 4.10). The

damage image obtained using ART is also interestingly found to be skewed in one direction. This observation is consistent to both single and multi-frequency cases. Finally, the results show that the number of iterations required to converge to a constant image is significantly higher for the case of a cross shaped damage. This could be due to the square shape being less complicated than the cross shape with regards to sharp edges and general geometry.

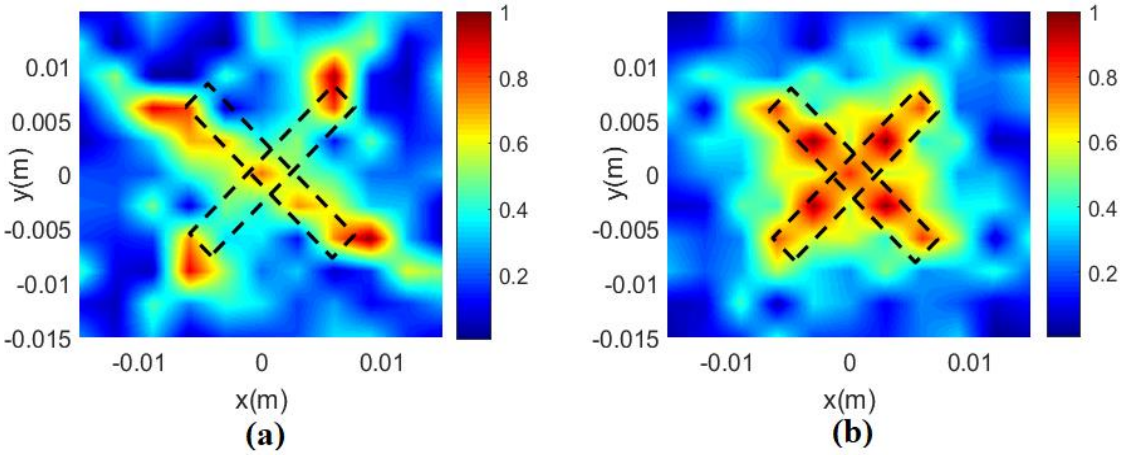

Figure 4.9: Damage reconstruction of a cross shaped damage using ART, for a) Case i and b) Case ii. Dashed lines indicate the true geometry of damage

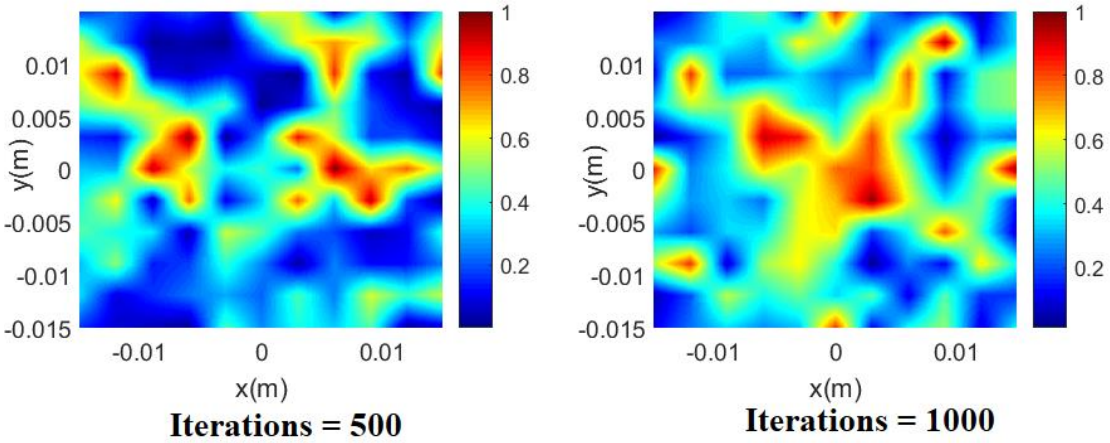

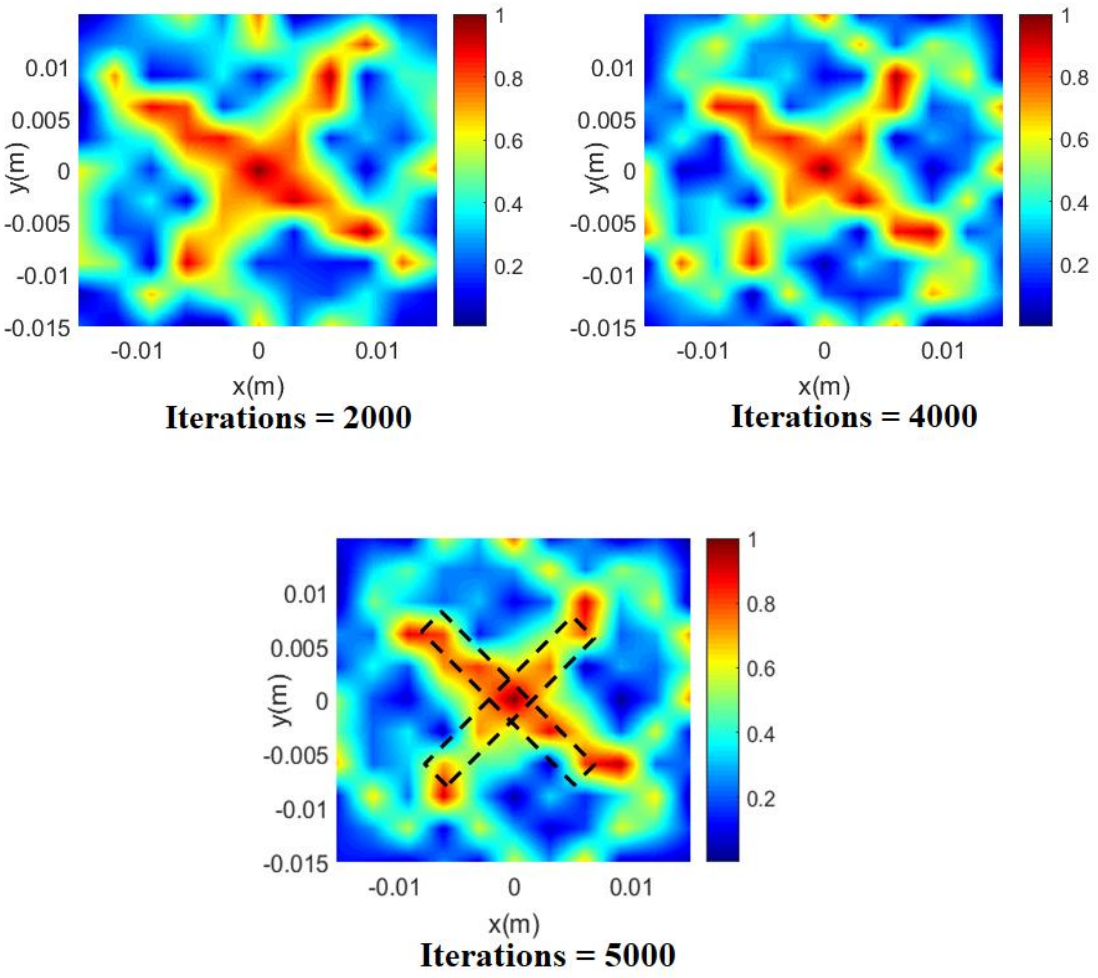

Figure 4.10: Iterations of ART for a cross shaped damage – 32 transducers with multi-frequency data (180 kHz, 200 kHz, and 220 kHz). Dashed lines indicate true geometry of damage

4.4.4. Off-centre circular damage

Finally, a circular damage that was offset from the centre of the transducer configuration was examined using the two aforementioned inverse methods. In this case, a circular damage of diameter 12 mm was located 20 mm away from the centre of the circular transducer configuration as shown in Fig. 4.11. This damage case too, is examined for the same three conditions as the above two cases. Namely, i) 32 transducers with a single frequency, ii) 64 transducers with a single frequency, and iii) 32 transducers with multiple frequencies.

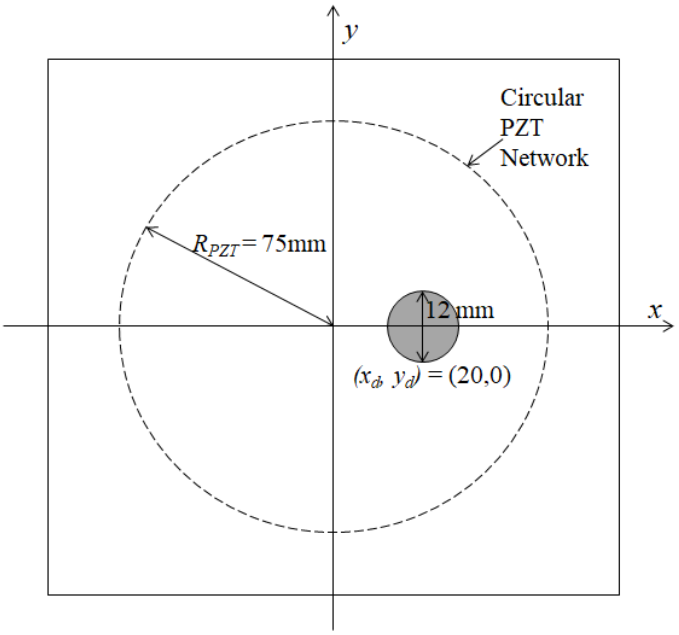

Figure 4.11: Schematic of the geometry, location and dimensions of the off-centre circular shaped thickness reduction damage

Least squares method

The results obtained using the least squares method, show that the off-centre location of the damage is predicted to great accuracy in both the single frequency (Figs. 4.12a and 4.12b) and the multi-frequency (Fig. 4.12c) cases. Additionally, both the location and dimensions of the damage seem to be accurately predicted, even with a 32 transducer system. The 64 PZT system (Fig. 4.12b) seems to result in the best image quality for this damage case. However, the multi-frequency case (Fig. 4.12c) has a significantly improved image quality when compared to the 32 PZT single frequency case (Fig. 4.12a).

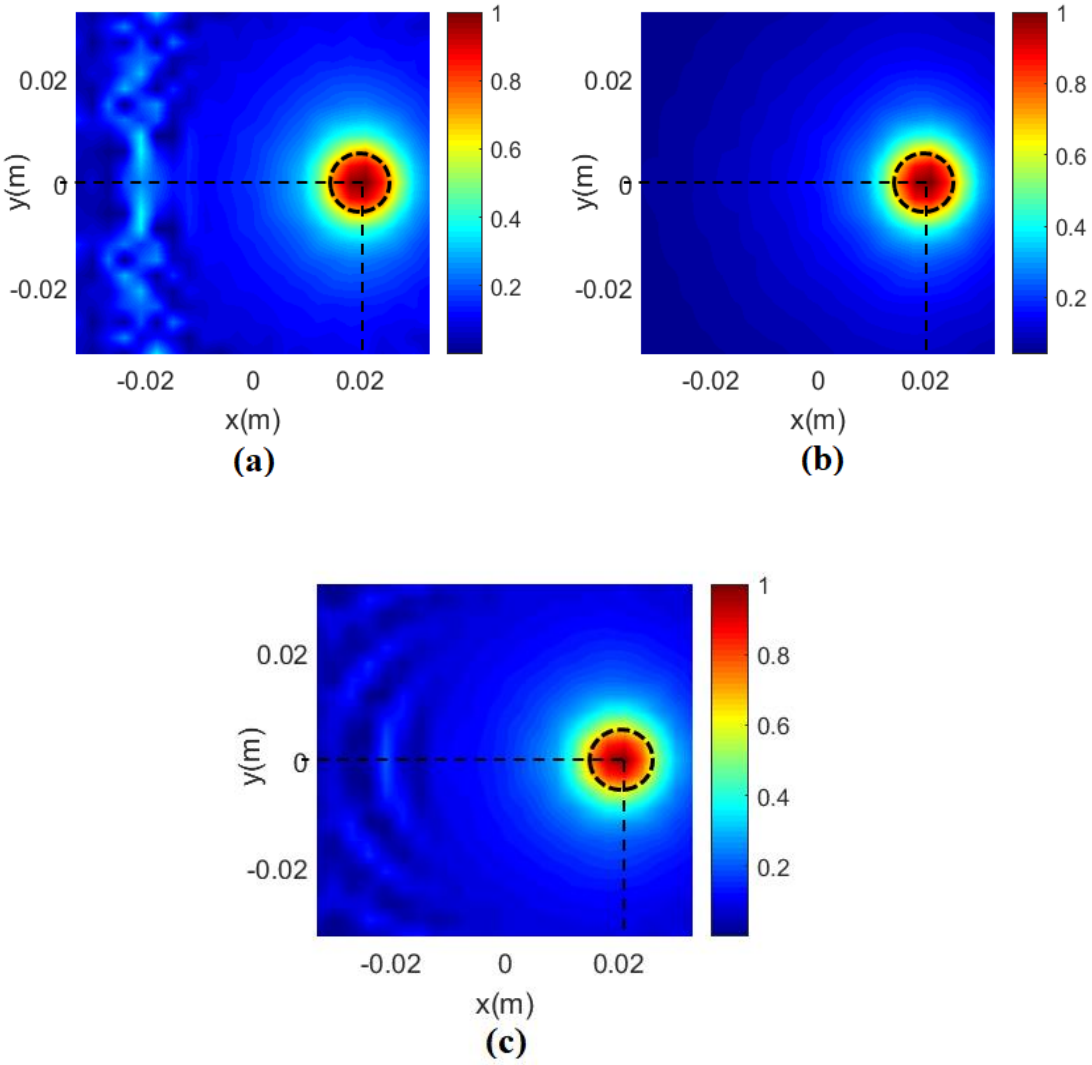

Figure 4.12: : Damage reconstruction of an off-centre circular shaped damage using least squares method for a) Case i, b) Case ii and (c) Case iii. Dashed lines indicate true geometry of damage

Algebraic Reconstruction Technique (ART)

The results obtained using ART for the off-centre circular shaped damage, are found to be comparable in accuracy to the results obtained using the least squares method. In this case too, the best image quality is obtained by using a 64 PZT system (Fig. 4.13b). However, in this case too, the 32 PZT multi-frequency

system (Fig. 4.14) has a slightly better image quality when compared to the 32 PZT single frequency case (Fig. 4.13a). Finally, the results show that the number of iterations required to converge to a constant image is relatively lesser for an off-centre circular shaped damage, when compared to a cross shaped damage located at the origin. It can thus be inferred that the number of iterations is highly dependent on the complexity of the damage shape. A circular shaped damage, regardless of its location, is found to take lesser number of iterations to converge, than a cross shaped damage. Other conclusions and inferences are presented in the following section.

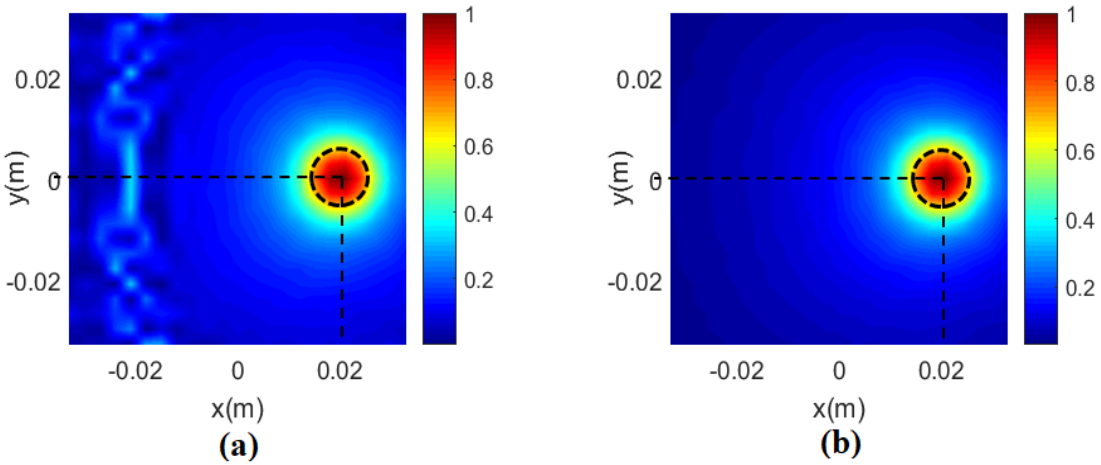

Figure 4.13: Damage reconstruction of an off-centre circular shaped damage using ART, for a) Case i and b) Case ii. Dashed lines indicate the true geometry of damage

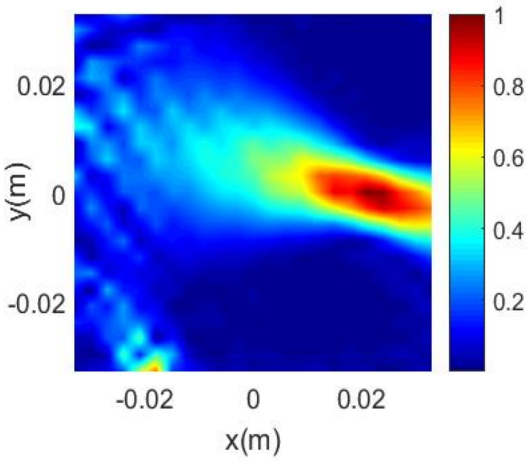

Iterations = 100

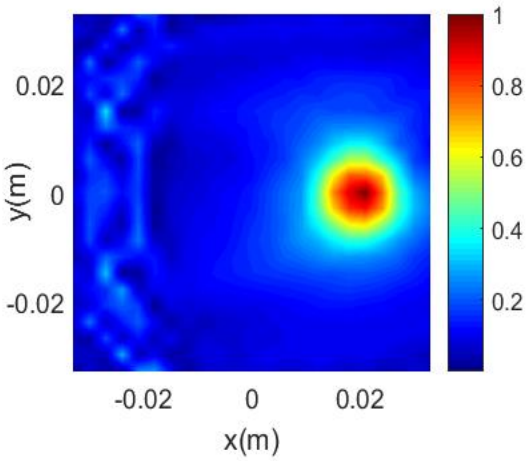

Iterations = 500

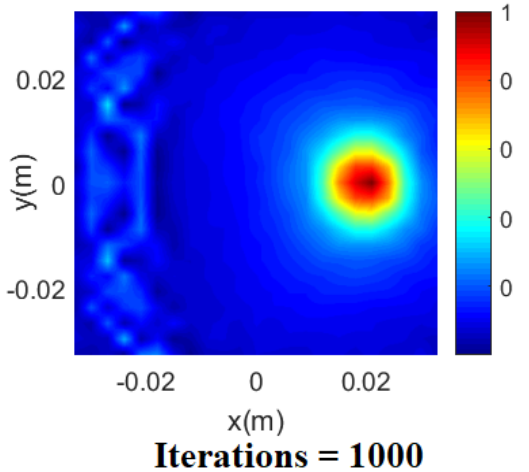

Iterations = 1000

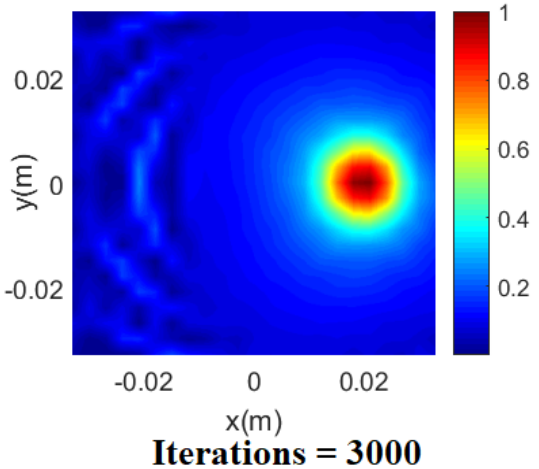

Iterations = 3000

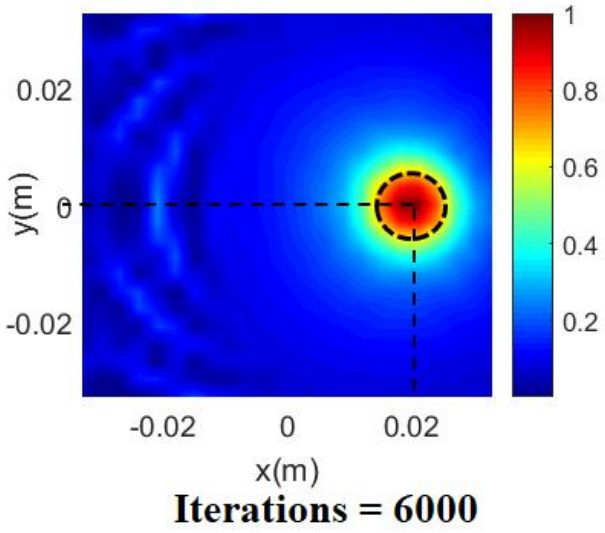

Figure 4.14: Iterations of ART for an off-centre circular shaped damage – 32 transducers with multi-frequency data (180 kHz, 200 kHz, and 220 kHz). Dashed lines indicate true geometry of damage

4.5. Discussions and Conclusions

Devaney and Dennison [9] showed that the effect of increasing frequencies is roughly the same as increasing the number of transducers by an equivalent factor. That is, taking two central frequencies for each transducer is the same as having twice the number of transducers in the system. Hence, the multi-frequency cases in this paper are equivalent roughly to 32 x 3 = 96 transducers. Thus, they are indeed expected to have a better performance than the single frequency case with 64 transducers. However, the "equivalency" might not hold in this case as the model proposed by Devaney and Dennison works with multiple central frequencies, whereas the multiple frequencies in this paper are non-central frequencies within the same scattered wave field.

It can also be observed that the pattern and grid spacing of the numerical Green's functions plays a very important role in the prediction of damage dimensions. For instance, a grid spacing of 2.5 mm will fail to adequately capture a square of size 12 mm located at the origin. This is because the boundary of the damage falls between 2 grid points, and hence, this feature cannot be captured adequately. This could also be the case for damages that have curved boundaries, such as a circular shape, unless the grid spacing is narrow enough to capture the curvature.

One important observation of note was that the value of the damage parameter at the origin was taken as the mean of the surrounding points in all the damage cases. This was due to the unusually high value of the parameter at this point.

Overall, it has been shown that the multi-frequency approach to damage reconstruction is a very feasible tool for improving the quality of the reconstructed damage image, and at the same time, significantly reducing the number of transducers. While ART has shown to have a slightly better performance when compared to the Least Squares method, the least squares method was found to be more computational efficient. The ART, on the other hand, allows for iterations in the damage image reconstruction, which is very helpful if locating the damage is of primary importance and reconstructing the detailed shape of the damage is not of immediate interest.

References

1. Doebling S.W, Farrar C.R, Prime M.B, *A summary review of vibration based damage identification methods*, 1998
2. Doherty, J. E., 1987, Nondestructive Evaluation, Chapter 12 in *Handbook on Experimental Mechanics*, A. S. Kobayashi Edt., Society for Experimental Mechanics, Inc.
3. Raghavan A, Cesnik C.E..S. Review of Guided Wave Structural Health Monitoring, *The Shock and Vibration Digest* 2007;
4. C.H.Wang and L.R.F. Rose, Plate-wave Diffraction Tomography for structural health monitoring, *Ann. Rev. QNDE*, Volume 22, pp. 1615-1622, 2003
5. A.H Rohde, L.R.F. Rose, M. Veidt, C.H.Wang, Two Inversion Strategies for Plate Wave Diffraction Tomography, *Materials Forum Volume* 33, 2009
6. Veidt, M, Rohde, AH, Ng, CT, Hames, S. Imaging laminar damage using plate wave ultrasonics and proposed methodology for designing optimal transducer networks. *Proceedings of the 2nd Asia-Pacific Workshop on SHM, Melbourne, Australia*. 2008
7. Ng, CT, Veidt, M, Rajic, N. Integrated piezoceramic transducers for imaging damage in composite laminates. *In Proceeding of SPIE*, 7493:74932M-1-8. 2009
8. Devaney, A. J., & Dennison, M. (2003). Inverse scattering in inhomogeneous background media. *Inverse Problems*, 19(4):855-870.

9. Dennison, M.L. and Devaney, A.J., 2004. Inverse scattering in inhomogeneous background media: II. Multi-frequency case and SVD formulation. *Inverse Problems*, *20*(4), p.1307.
10. K.J.Nicholson, C.H Wang, Improved near-field radar cross-section near field technique, *IEEE Antennas Wirel. Propag. Lett. 16*, pp. 1103-1106, 2009
11. Chan E., Rose L.R.F, Wang C.H, An extended diffraction tomography method for quantifying structural damage using numerical Green's functions, *Ultrasonics*, 2015
12. Pudipeddi, G.T., Ng, C.T. and Kotousov, A., 2018. Effect of central and non-central frequency components on the quality of damage imaging. *Journal of Civil Structural Health Monitoring*, *8*(1), pp.49-61
13. Belanger, P., Cawley, P., & Simonetti, F. (2010). Guided wave diffraction tomography within the born approximation. *IEEE transactions on ultrasonics, ferroelectrics, and frequency control*, 57(6):1405-1418.
14. Malyarenko, E. V., & Hinders, M. K. (2001). Ultrasonic Lamb wave diffraction tomography. *Ultrasonics*, *39*(4):269-281.
15. Rose, L. F., & Wang, C. H. (2010). Mindlin plate theory for damage detection: imaging of flexural inhomogeneities. *The Journal of the Acoustical Society of America*, 127(2):754-763.
16. Ng, C. T. (2015). A two-stage approach for quantitative damage imaging in metallic plates using Lamb waves, 8(4):821-841
17. Twomey S 1996 *Introduction to the Mathematics of Inversion and Remote Sensing and Indirect Measurements* (New York: Dover)

18. Gordon, R., Bender, R. and Herman, G.T., 1970. Algebraic reconstruction techniques (ART) for three-dimensional electron microscopy and X-ray photography. *Journal of theoretical Biology*, *29*(3), pp.471-481.
19. Simonetti, F. and Huang, L., 2008. From beamforming to diffraction tomography. *Journal of Applied Physics*, *103*(10), p.103110.
20. Huthwaite, P. and Simonetti, F., 2013. High-resolution guided wave tomography. *Wave Motion*, *50*(5), pp.979-993.
21. Huthwaite, P. and Simonetti, F., 2011. High-resolution imaging without iteration: A fast and robust method for breast ultrasound tomography. *The Journal of the Acoustical Society of America*, *130*(3), pp.1721-1734.
22. Huthwaite, P., 2014. Evaluation of inversion approaches for guided wave thickness mapping. *Proceedings of the Royal Society A: Mathematical, Physical and Engineering Sciences*, *470*(2166), p.20140063.

Chapter 5

5. Conclusions and recommendations

5.1. Conclusions

The thesis has studied the properties of Lamb wave scattering and has proposed a framework to enhance the application of LWDT as a non-destructive evaluation technique. The research has particularly focussed on improving the LWDT algorithm through the inclusion of a multi-frequency framework. The results have shown that this significantly reduces the logistics involved in gathering data for the LWDT process. Inclusion of multi-frequency data makes a significant contribution to the advancement of LWDT as a feasible and accurate technique for the damage identification of plate-like structures.

The major outcomes and research contributions of this study are listed below.

1. The scattering and mode conversion of a Lamb wave at the delaminations in a $[-45/45/0/90]_S$ QI composite laminate have been studied in detail. From the results of the SDPs, it has been shown that the fibre orientation of the outer laminae have a significant influence on both A_0 scattered and A_0-S_0 mode converted Lamb wave patterns. It has also been shown that the amplitudes of A_0 scattered and A_0-S_0 mode converted Lamb waves have an increasing trend with the delamination size. Finally, the effect of the through-thickness location of the delamination on the A_0 scattered and

A_0-S_0 mode converted Lamb wave has been demonstrated using the SDP. Overall, this study has made a significant contribution in understanding the behaviour of Lamb waves in the context of mode conversion.

2. This study has investigated the performance of LWDT in reconstructing different shapes of damage using central and non-central frequencies. The results have shown that the non-central frequencies are capable of reconstructing damage using LWDT. This means that these multi-frequency can provide additional information in the LWDT algorithm when they are used in conjunction with the central frequency data. One of the main inferences of this study is that the symmetric frequencies on either side of the central frequency have different results in the damage image reconstruction. This can aid in recognising the most efficient interval for studying multi-frequency approaches of damage image reconstruction.
3. This study has proposed a multi-frequency approach to reconstruct the damage image. The use of the multi-frequency data can improve the quality of the reconstructed image, and significantly reduce the number of transducers. The results have shown that the ART method performs marginally better than the Least Squares method for predicting the shape and size of damage. However, the least squares method was found to be more computationally efficient than ART. The ART also allows for iterations in the damage image reconstruction. This can be very helpful if the shape and dimensions of the damage being inspected are not as important as the location of the damage.

5.2. Recommendations

This study has provided knowledge and inputs for future research in the area of LWDT. Some of the directions, from which the findings of this research can be taken forward, are listed below:

1. While the mode-conversion and SPDs of incident A_0 Lamb wave and the mode converted $A_0 - S_0$ waves were studied; further research to see the significance of these mode-converted waves in the scattered wave-field and their ability to aid in the reconstruction of damage can be studied in detail.
2. In addition to multiple frequencies can provide additional information to the LWDT algorithm. Thus, possibly resulting in still further reduction in the number of transducers and a much higher resolution of damage.
3. The effect of the number of frequencies included in the multi-frequency approach on the quality of damage can have a significant impact on the performance of the LWDT algorithm. Increasing the number of frequencies beyond a point could lead to only a marginal increase in the quality of damage, while significantly increasing the computational costs. The frequency interval that would lead to the optimal quality of image can also be studied.
4. Studying the multi-frequency approach in the context of non-linear guided waves would go a long way in improving the LWDT algorithm. This is because of the higher sensitivity of non-linear guided waves to damage size. Hence extending the method to include non-linear waves could open up the algorithm to a wider range of damages and materials.